PRE-COSTAR FOS APERTURE THROUGHPUTS FOR MIS-CENTERED TARGETS DERIVED FROM PSF MODELS

I. N. Evans
Space Telescope Science Institute

FOS Instrument Science Report CAL/FOS-107
November 1993

Abstract

Monochromatic pre-COSTAR aperture relative throughputs for the FOS have been computed from model point spread functions for point source targets that are mis-centered in the FOS apertures. Model aperture throughputs relative to a perfectly centered point source target are presented for each of the non-occulting FOS apertures. Plots of the maximum and minimum aperture relative throughput versus radius are presented for use when the position angle of the offset target vector is unknown, and in the form of contour plots of the aperture relative throughput versus offset X and Y for use when the precise offset is known. The model aperture relative throughputs agree with the the observational data except in the case of the 4.3 aperture, where the observed flux is lower than predicted for large target offsets.

I. Pre-COSTAR FOS Aperture Throughputs For Mis-centered Targets

FOS blue side and red side pre-COSTAR monochromatic aperture relative throughputs have been determined for mis-centered point source targets for each of the non-occulting FOS apertures from the model point spread functions (PSFs) described by Evans (1993). Relative aperture throughputs are computed at wavelengths of 1400Å, 2000Å, 2800Å, 4000Å, and 5000Å for the FOS blue side, and at wavelengths of 2000Å, 2800Å, 4000Å, 5600Å, and 7400Å for the FOS red side. The PSFs computed by Evans (1993) use the default aberrations and nominal focus for the date June 1, 1993.

The aperture relative throughput for a mis-centered point source target is defined as the ratio of the transmitted integrated flux from the mis-centered point source target to the transmitted integrated flux from a point source target that is perfectly centered in the aperture. The aperture relative throughputs are computed by summing the individual contributions of the pixels of the mis-centered PSF at each pixel position within the relevant FOS aperture, and dividing this value by the sum of the individual contributions of the pixels of a perfectly centered PSF at each pixel position within the relevant FOS aperture. Because of the fine pixel sampling of the PSFs, no correction for the presence of fractional pixels within a given aperture is applied. The apertures are assumed to be perfectly circular in the case of the circular apertures, and perfectly rectangular with sides aligned precisely in the X and Y directions for the rectangular apertures. The aperture sizes used are obtained from the PDB (Dressel & Harms, unpublished), except in the cases of the

4.3 and 0.25×2.0 apertures, where the Y extent (only) of the apertures is limited by the effective diode height and is assumed to be precisely 1″.43. The PDB values for the aperture areas do not agree (by up to $\sim 40\%$ for the blue side 0.1-PAIR and red side 0.1-PAIR-A apertures) with pre-flight measurements of Lindler, Bohlin, and Hartig (1985).

The aperture relative throughputs for each aperture are computed for a Monte Carlo sample of 1000 target positions drawn from a uniform random distribution covering a rectangular region centered at the aperture center, and extending in the X and Y directions to a distance of $\pm 150\%$ of the X and Y half-widths of the aperture, respectively.

II. Results

Aperture relative throughputs for mis-centered point source targets are summarized in Figure 1, where for each aperture the approximate maximum and minimum values of the aperture throughput relative to the aperture throughput of a perfectly centered point source target are plotted as a function of target radius from the aperture center. For each aperture, the envelope of the minimum and maximum aperture relative throughputs is determined by forming the histogram of the aperture relative throughputs computed from the Monte Carlo sample as a function of radius from the aperture center. The histogram is computed using 20 bins equally spaced from the center of the aperture to a radius of 150% of the aperture half width. The position angle dependence of the aperture relative throughputs is not plotted in Figure 1. Instead, the aperture relative throughput is azimuthally averaged in each radial histogram bin, and the minimum and maximum aperture relative throughput values determined. These values are then smoothed using a three point box-car filter, and the resulting envelope is plotted as a function of radius in Figure 1.

For the circular apertures, the differences between the minimum and maximum aperture relative throughputs shown in Figure 1 arises solely from the azimuthal asymmetry of the point spread functions at the FOS aperture positions. For the non-circular apertures, the differences between the minimum and maximum aperture relative throughputs are dominated by the dependence on the position angle of the offset vector of the mis-centered target from the aperture center, although there is also a contribution from the azimuthal asymmetry of the point spread functions. In the case of the square apertures, the upper envelope of the aperture relative throughput in Figure 1 corresponds approximately to target mis-centering offset along a diagonal of the aperture, while the lower envelope corresponds approximately to target mis-centering offset perpendicular to an aperture edge. Similarly, for the rectangular apertures, the upper envelope corresponds approximately to target mis-centering offset along the long dimension of the effective aperture size (the X direction for the 4.3 aperture, the Y direction for the 0.25X2.0 aperture), while the lower envelope corresponds approximately to target mis-centering offset in the perpendicular direction.

Examination of Figure 1 demonstrates that the aperture relative throughput exceeds unity for some target mis-centerings in the smallest apertures. This occurs because the pre-COSTAR

PSF at the location of the FOS apertures is not symmetric, and the position of the peak of the intensity distribution is not coincident with the center location of the PSF. The total flux sampled through a small aperture located at the center position of the PSF is less than the total flux sampled through the same aperture located at the position of the peak of the PSF. This effect is negligible for the 0.3 and larger apertures because the core of the PSF is included in the region sampled by one of these apertures located at the center position of the PSF.

Also plotted in Figure 1 for comparison are the observed throughput ratios for mis-centered targets (Bohlin 1993) for those aperture where such data exist. Inspection of the figure shows that while the models fit the data for most of the apertures where observations exist, there is a discrepancy in the case of the 4.3 aperture, where the data tend to fall below the lower envelope of the models for reasons that are unclear. The observational data for the 4.3 aperture are obtained by comparing the total flux measured for a given Y displacement of the target with the total flux for the same target with no Y displacement. No correction is applied for the displacement of the target in X from the aperture center. This is equivalent to assuming that the ratio of the target flux for a point source centered at (X, Y) divided by the target flux for a point source centered at (X, 0) is identical to the ratio of the target flux for a point source centered at (0, Y) divided by the target flux for a point source centered at (0, 0). Although this assumption is not rigorously correct, it is accurate to better than $\sim 3\%$ for almost the entire X range of the 4.3 aperture. The discrepancy between the models and the observational data for the 4.3 aperture could arise from oversubtracting the background from the observational data, or from overestimating the relative intensity of the wings of the PSF models.

Contour plots of the aperture relative throughputs for point source targets as a function of target position within the aperture are presented in Figure 2. To construct this figure, a Delaunay triangulation is computed from the Monte Carlo sample of aperture relative throughputs, and then uniformly gridded using Akima's quintic polynomials. This operation is repeated for each detector, aperture, and wavelength combination. However, only the contour plots for the wavelengths 1400Å and 2800Å on the blue side, and 2800Å and 5600Å on the red side, are shown in Figure 2. The contours in Figure 2 are drawn at relative throughput values of 0.2, 0.4, 0.6, 0.8, 0.9, 0.95, and 1.0 with solid lines, and 1.05, 1.1, 1.2, and 1.4 with dotted lines. In principle, the 1.0 relative throughput contour should intersect the (X, Y) = (0, 0) offset location; in practice, effects arising from the Monte Carlo sampling and the regridding cause small deviations.

Although the gridded surface is fit by a smooth function, the relatively sparse Monte Carlo sampling can result in some anomalies in the final contoured data. A typical example of such an anomaly may be seen on the blue side plots for the 0.1-PAIR aperture, where there is an apparent "hole" in the throughput at (X, Y) $\approx$ (0.045, -0.005). Another form of anomaly may be seen in the red side plots for the 0.25X2.0 aperture, where the extrapolation of the gridding to large negative Y offsets and large X offsets has produced spurious contours. Such features are easy to identify by visual inspection, so no attempt has been made to artificially edit or smooth

the data to remove these blemishes. The pixel spacing of the model PSFs becomes significant for the smallest apertures. For example, the model PSF pixel spacing is $\sim 5\%$ of the width of the 0.1-PAIR apertures. The X and Y offset positions of the Monte Carlo sample are implicitly quantized by the model PSF pixel spacing. This results in an artificially irregular appearance for the contours in Figure 2 for the 0.1-PAIR apertures.

References

Evans, I. N. 1993, FOS Instrument Science Report CAL/FOS-104
Lindler, D. J., Bohlin, R. C., & Hartig, G. F. 1985, FOS Instrument Science Report CAL/FOS-019

Figure Captions

Fig. 1 — Aperture relative throughputs as a function offset radius for mis-centered point source targets. Each panel is identified by detector and aperture id. The minimum and maximum limits of the envelope histogram at wavelengths 1400Å, 2000Å, 2800Å, 4000Å, and 5000Å for the blue detector, and at wavelengths 2000Å, 2800Å, 4000Å, 5600Å, and 7400Å for the red detector, are symbolized by plus signs, stars, diamonds, triangles, and squares, respectively. Where available, observational measurements are marked by filled circles.
Fig. 2 — Aperture relative throughput contours as a function of target X and Y offset. Each panel is identified by detector, aperture id, and wavelength. The solid contours are drawn at aperture relative throughput values of 0.2, 0.4, 0.6, 0.8, 0.9, 0.95, and 1.0. Dotted contours are drawn at aperture relative throughput values of 1.05, 1.1, 1.2, and 1.4.

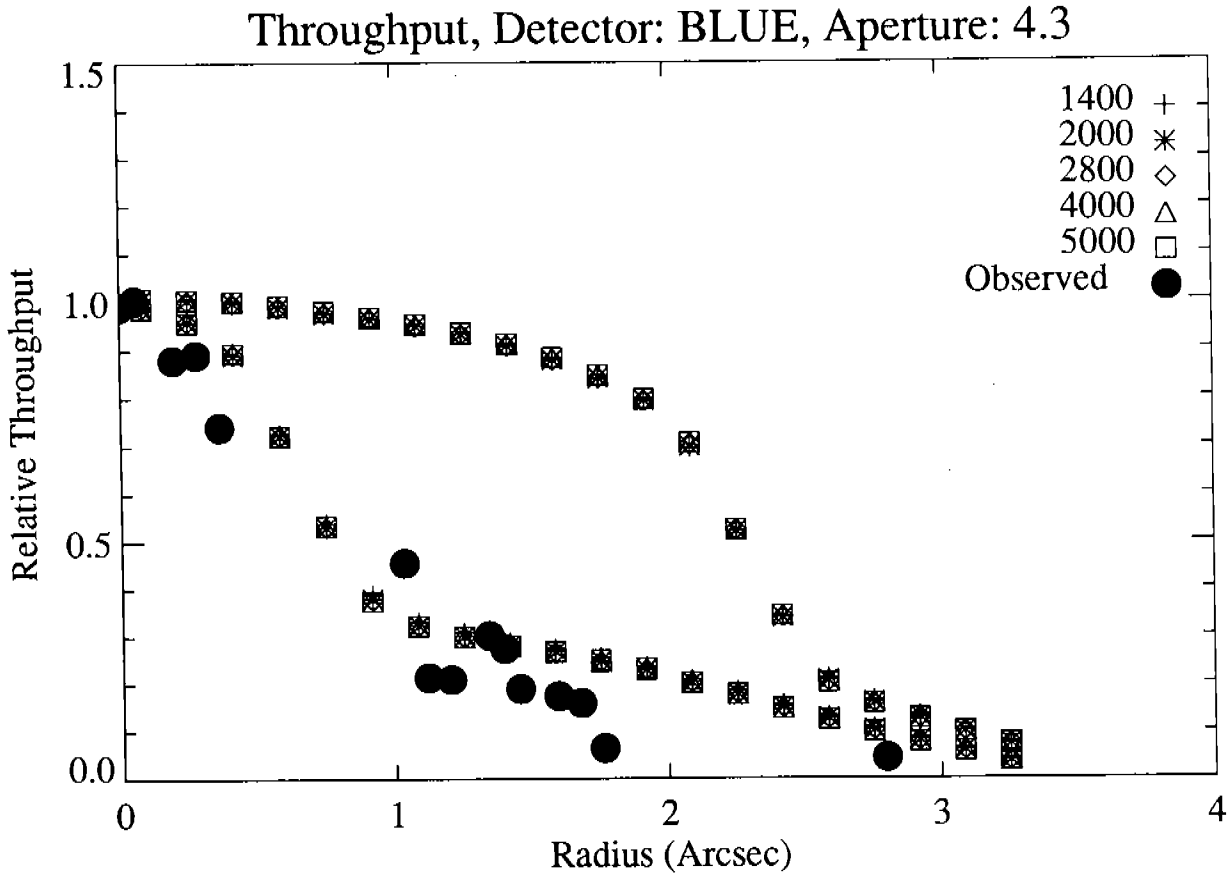
Throughput, Detector: BLUE, Aperture: 4.3
1400 +
2000 ✳
2800 ◇
4000 △
5000 □
Observed
Relative Throughput
1.5
1.0
0.5
0.0
0
1
2
3
4
Radius (Arcsec)

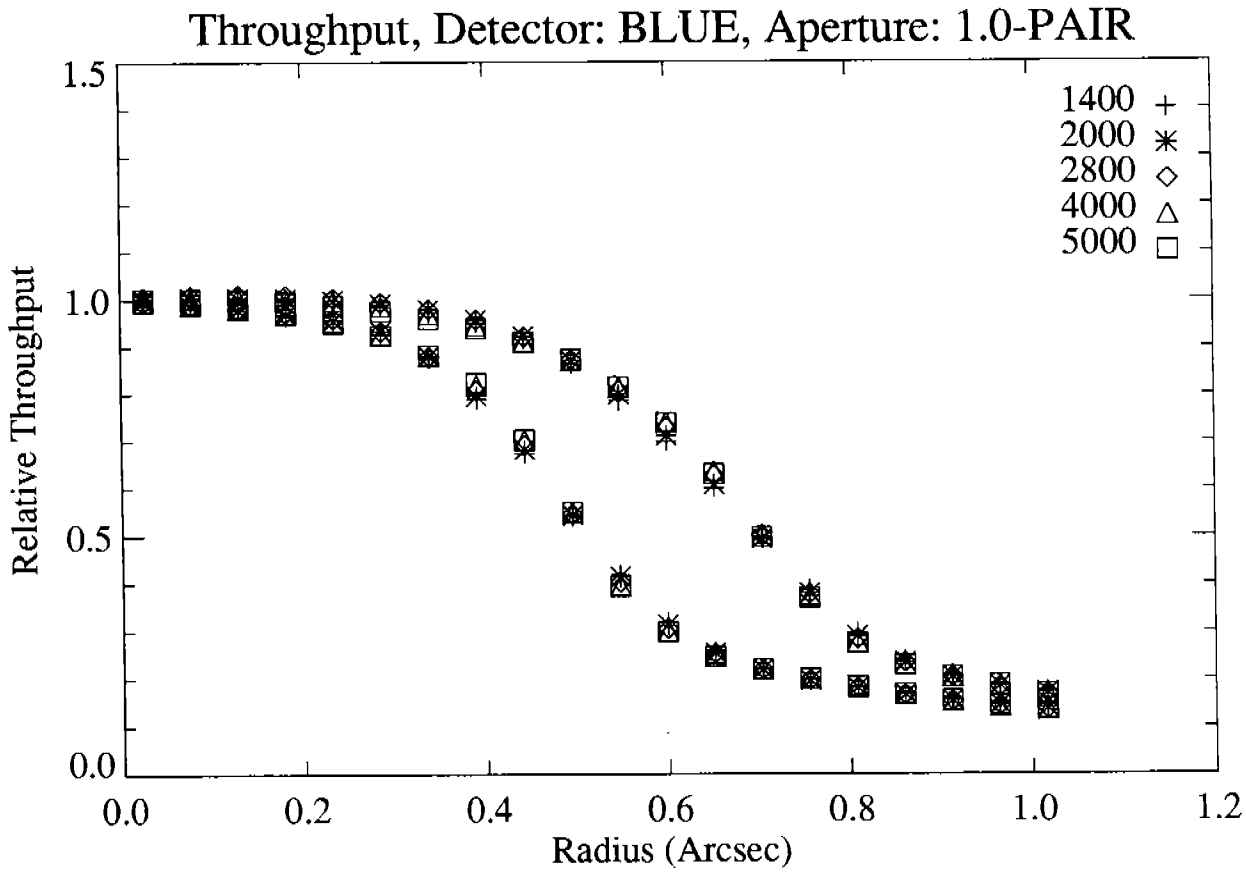
Throughput, Detector: BLUE, Aperture: 1.0-PAIR
1400 +
2000 ✳
2800 ◇
4000 △
5000 □
Relative Throughput
1.5
1.0
0.5
0.0
0.0
0.2
0.4
0.6
0.8
1.0
1.2
Radius (Arcsec)

Figure 1

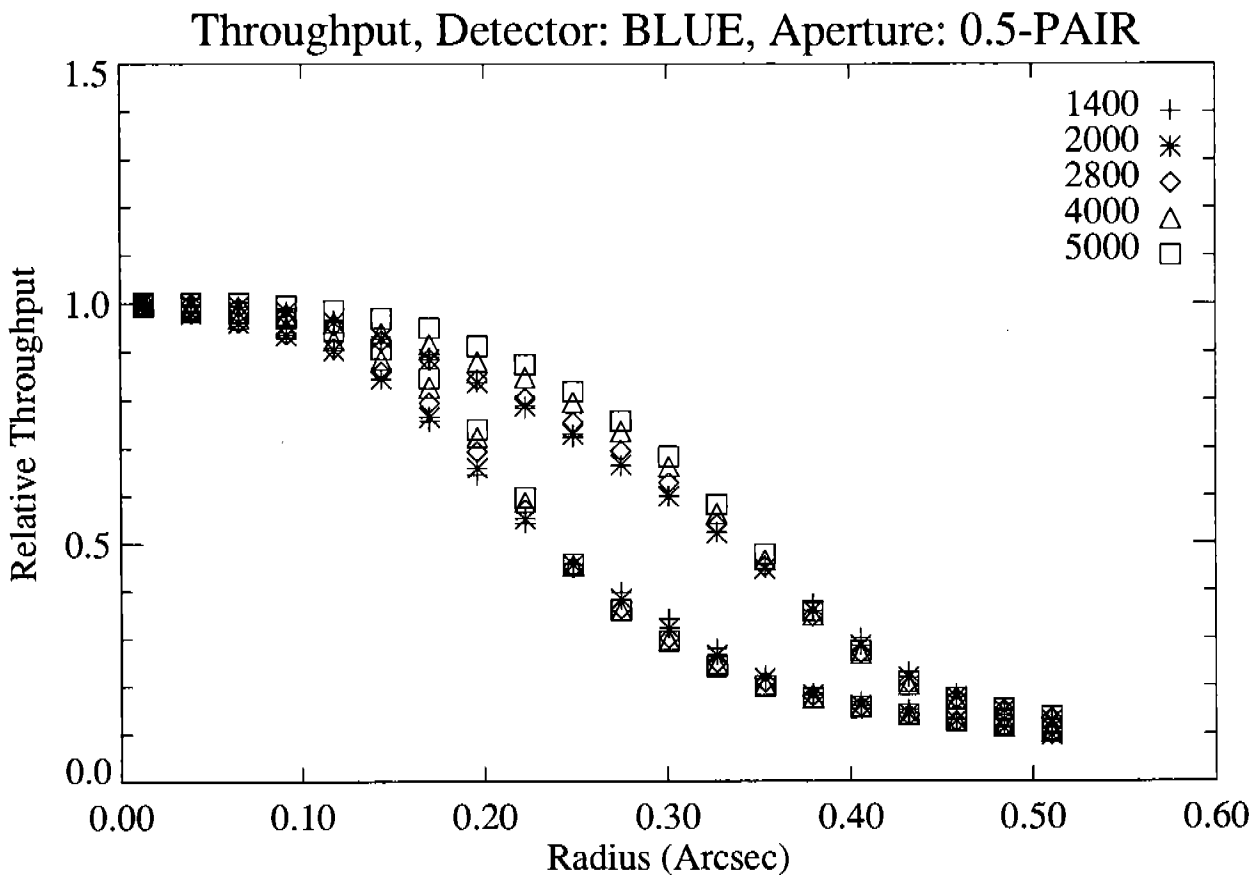

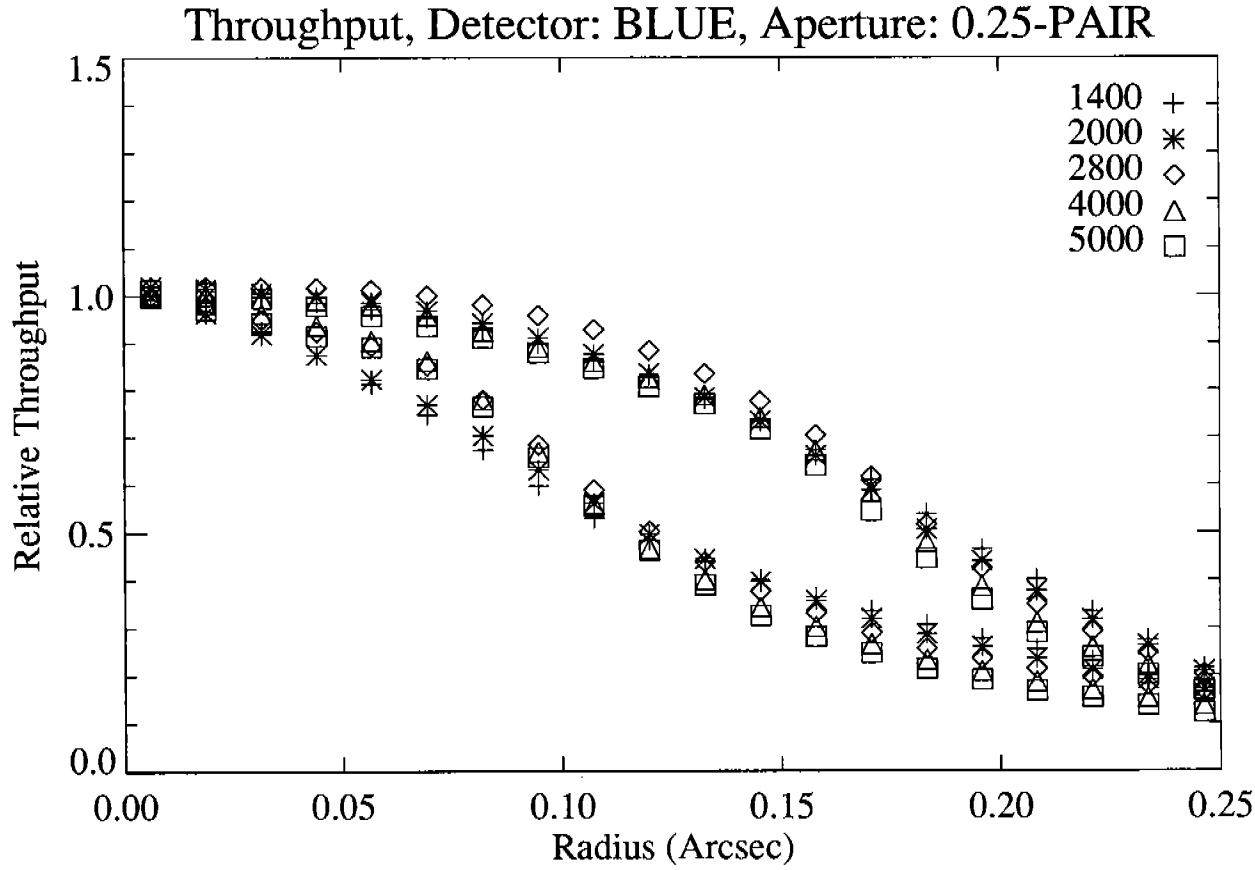

Figure 1 (Continued)

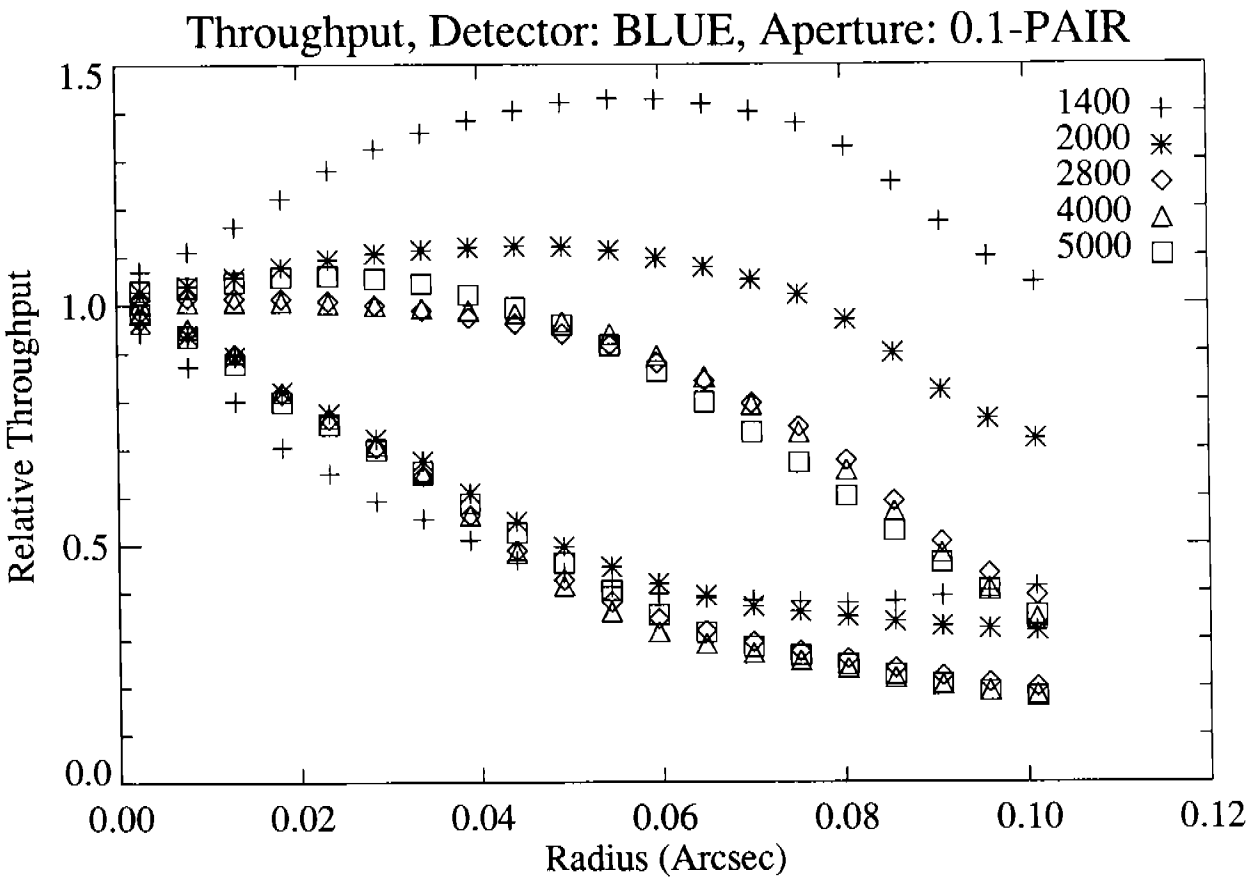

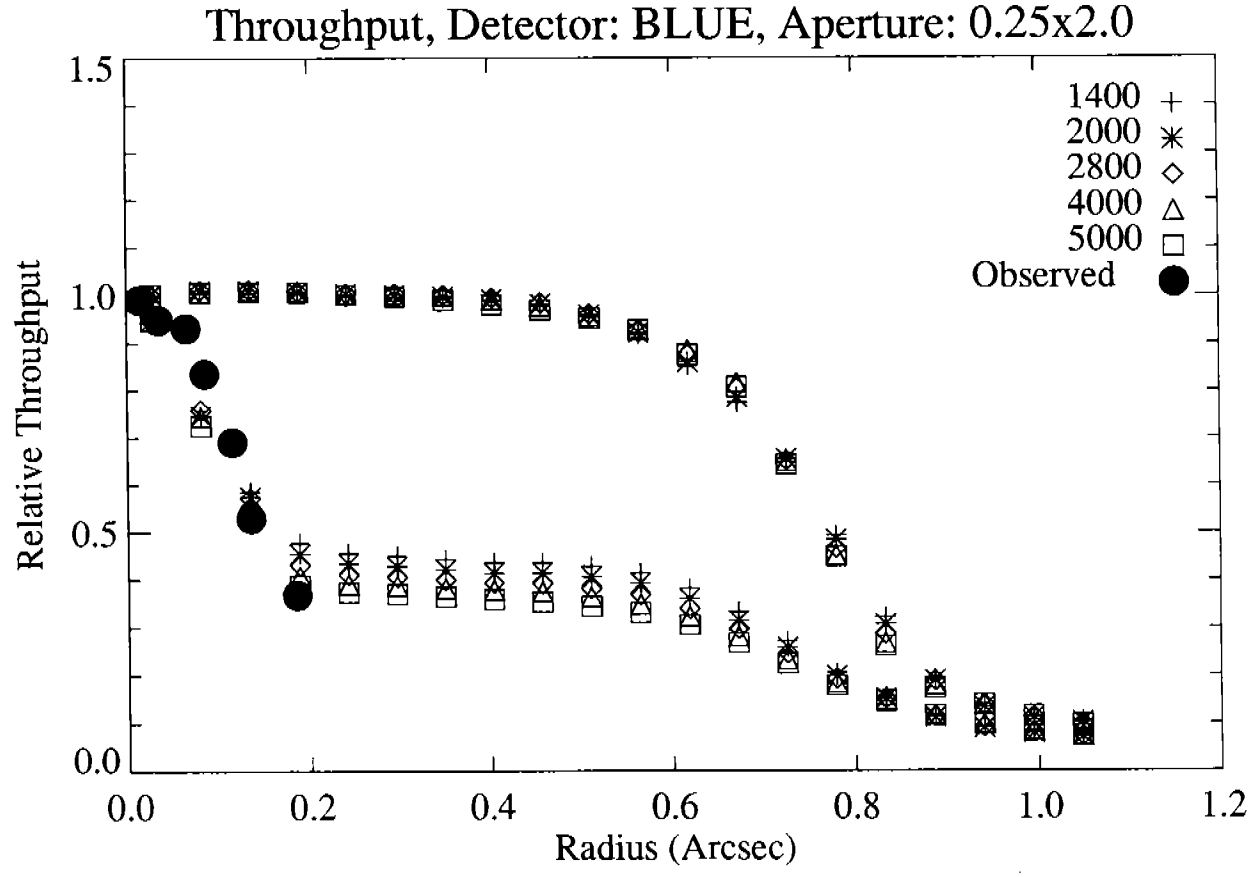

Figure 1 (Continued)

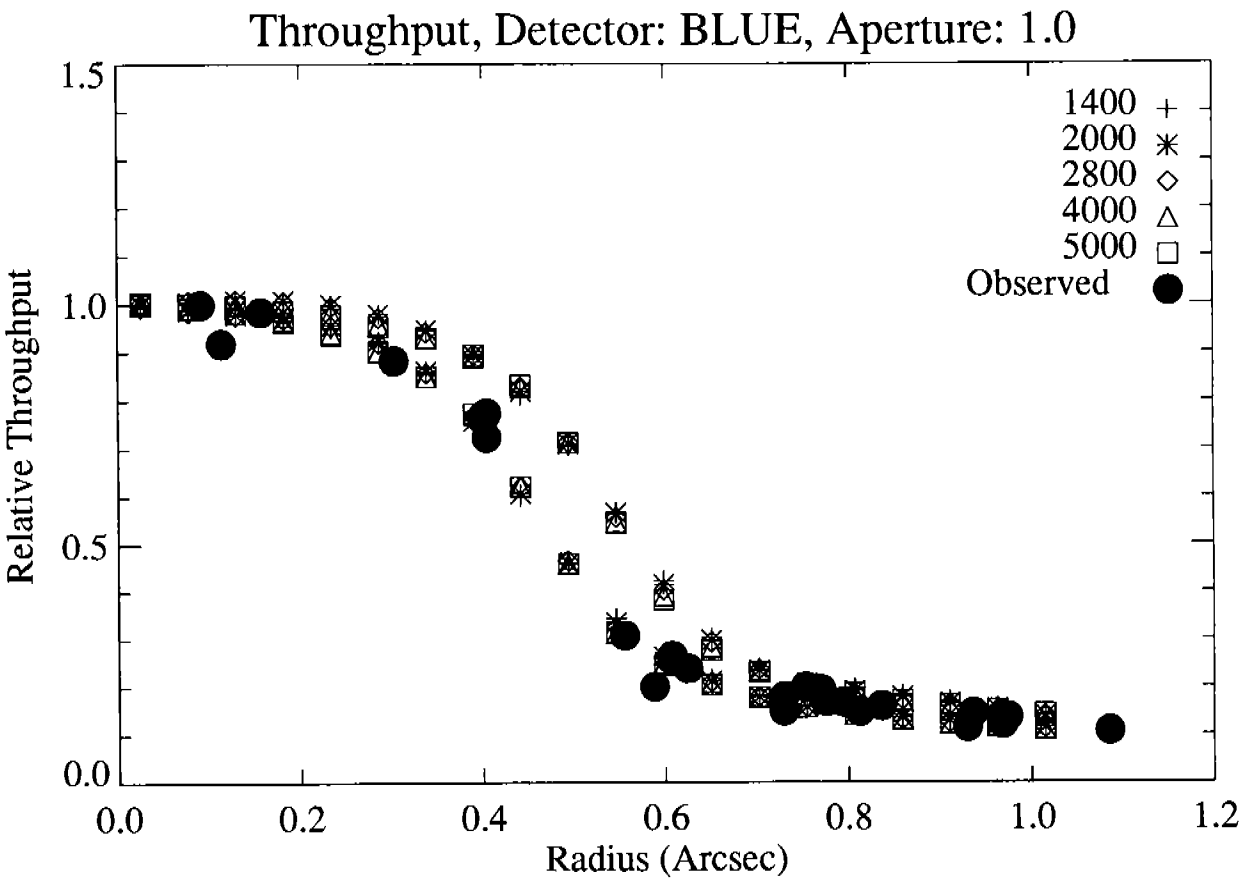

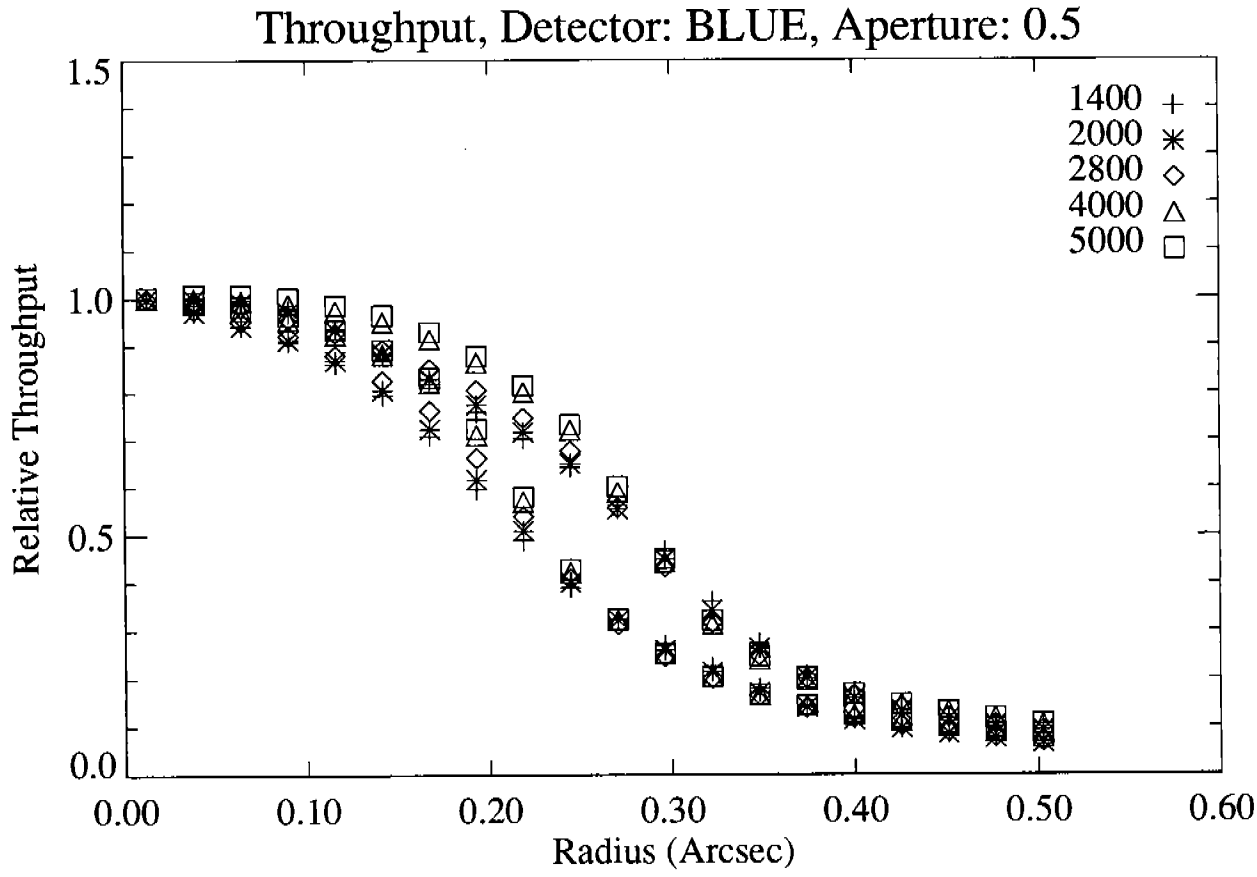

Figure 1 (Continued)

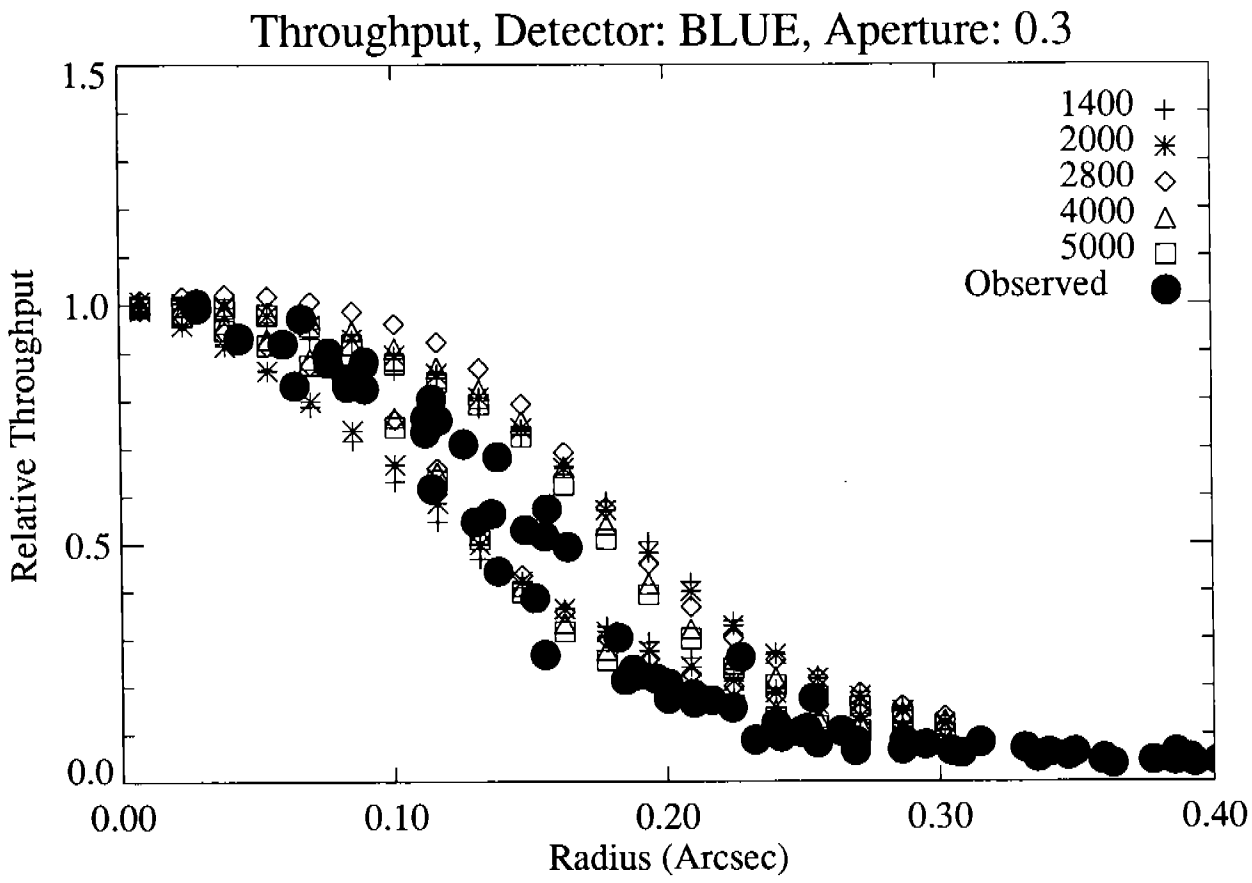

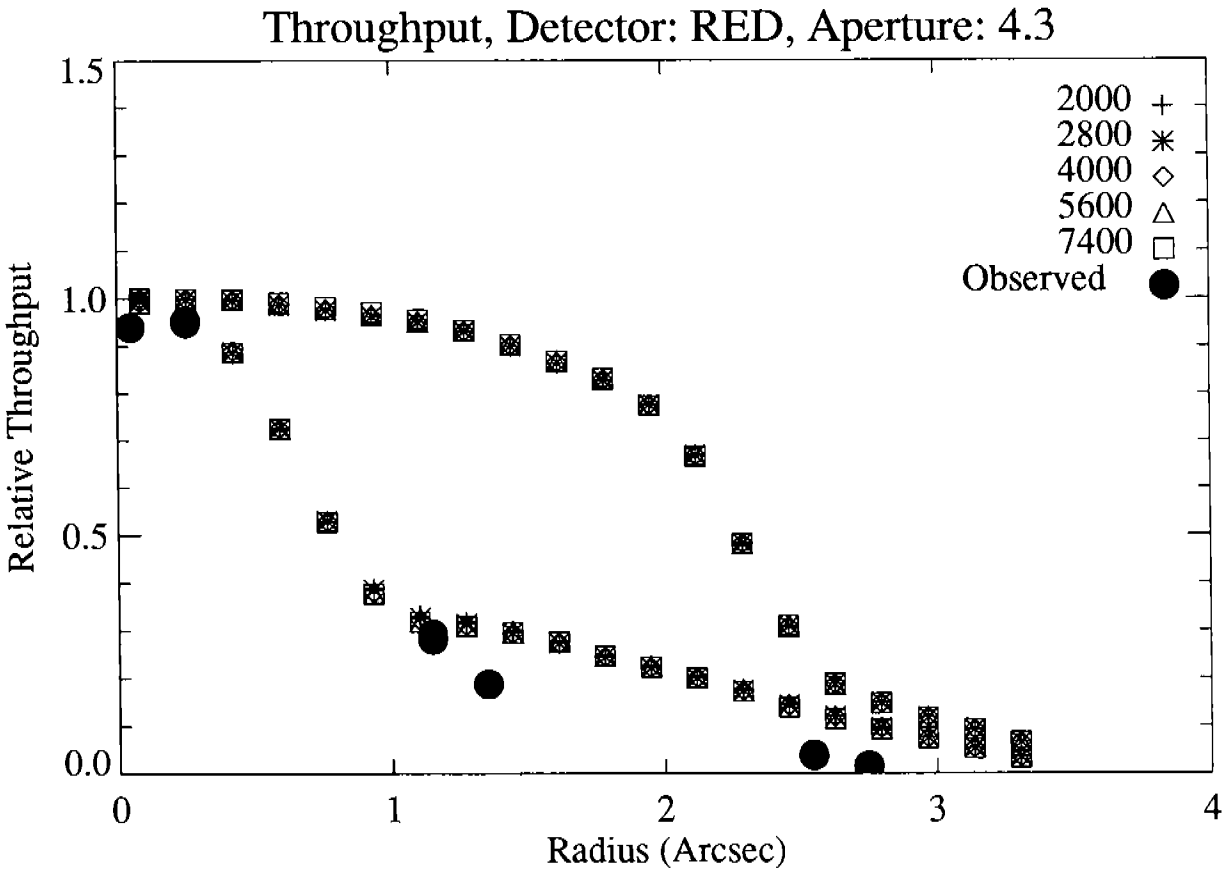

Figure 1 (Continued)

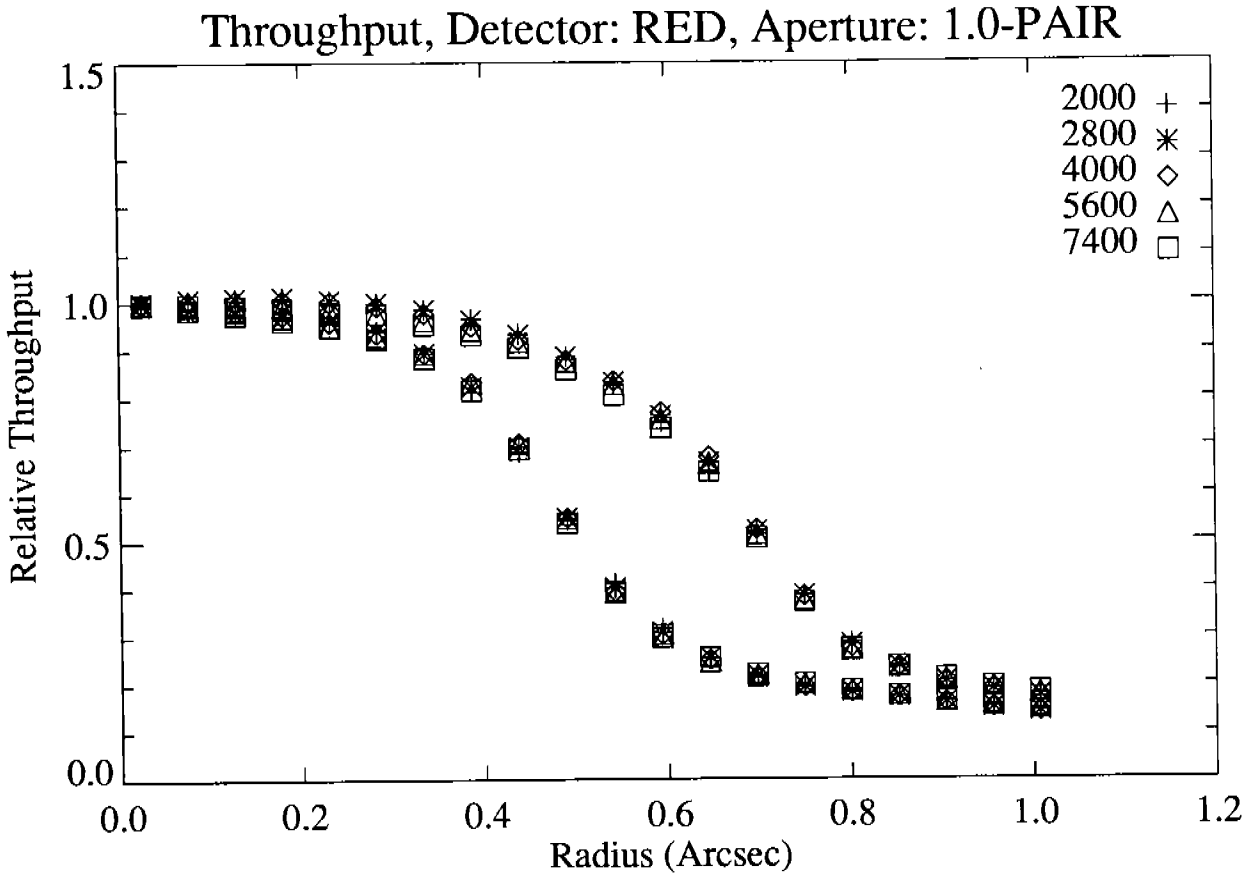

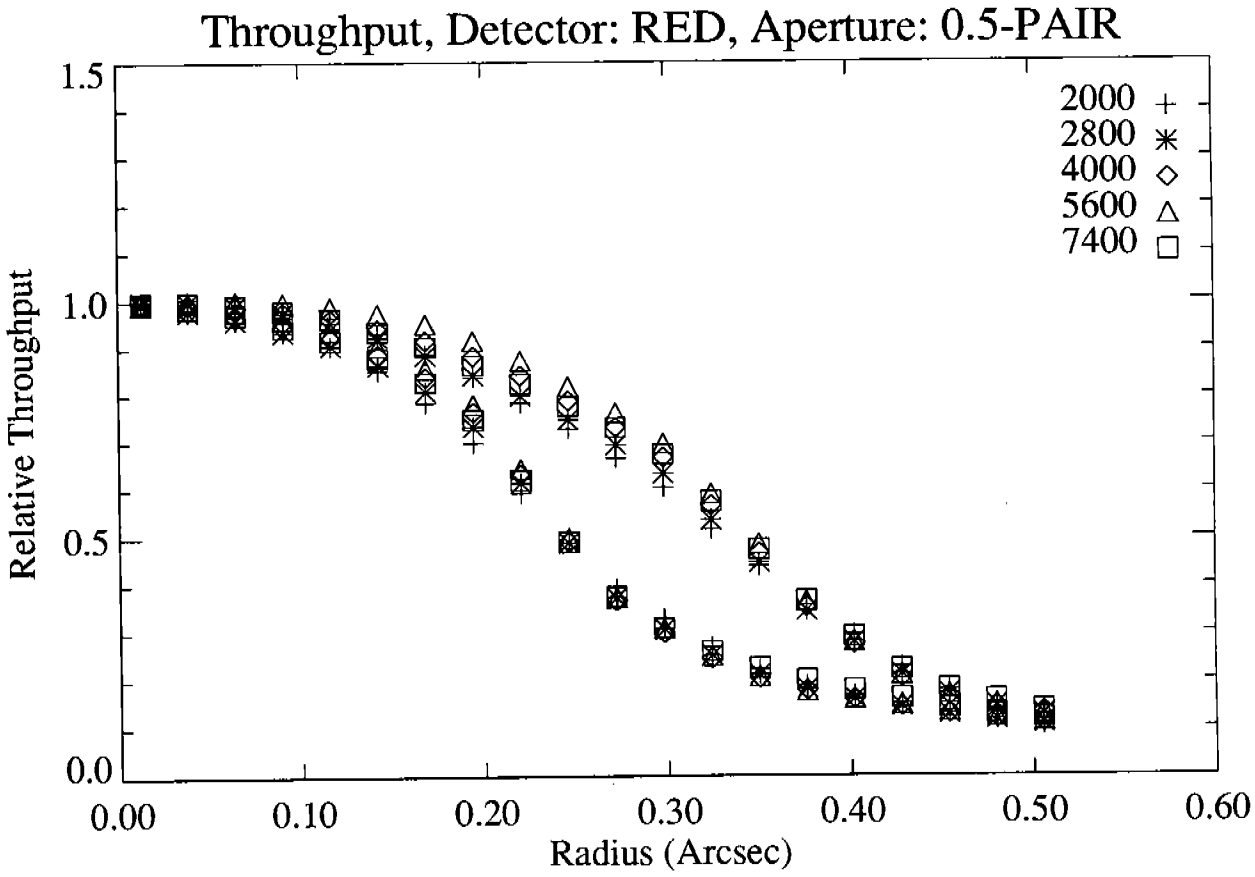

Figure 1 (Continued)

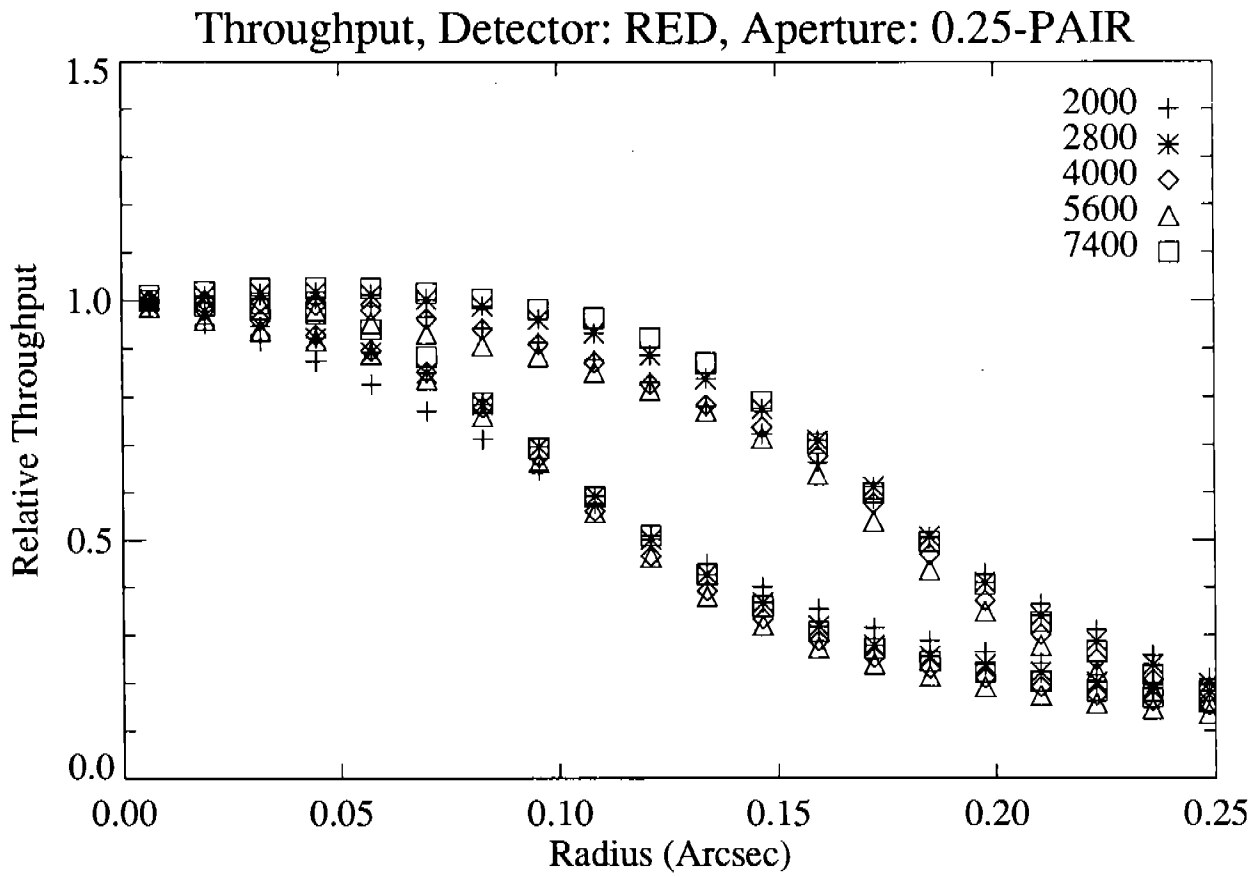

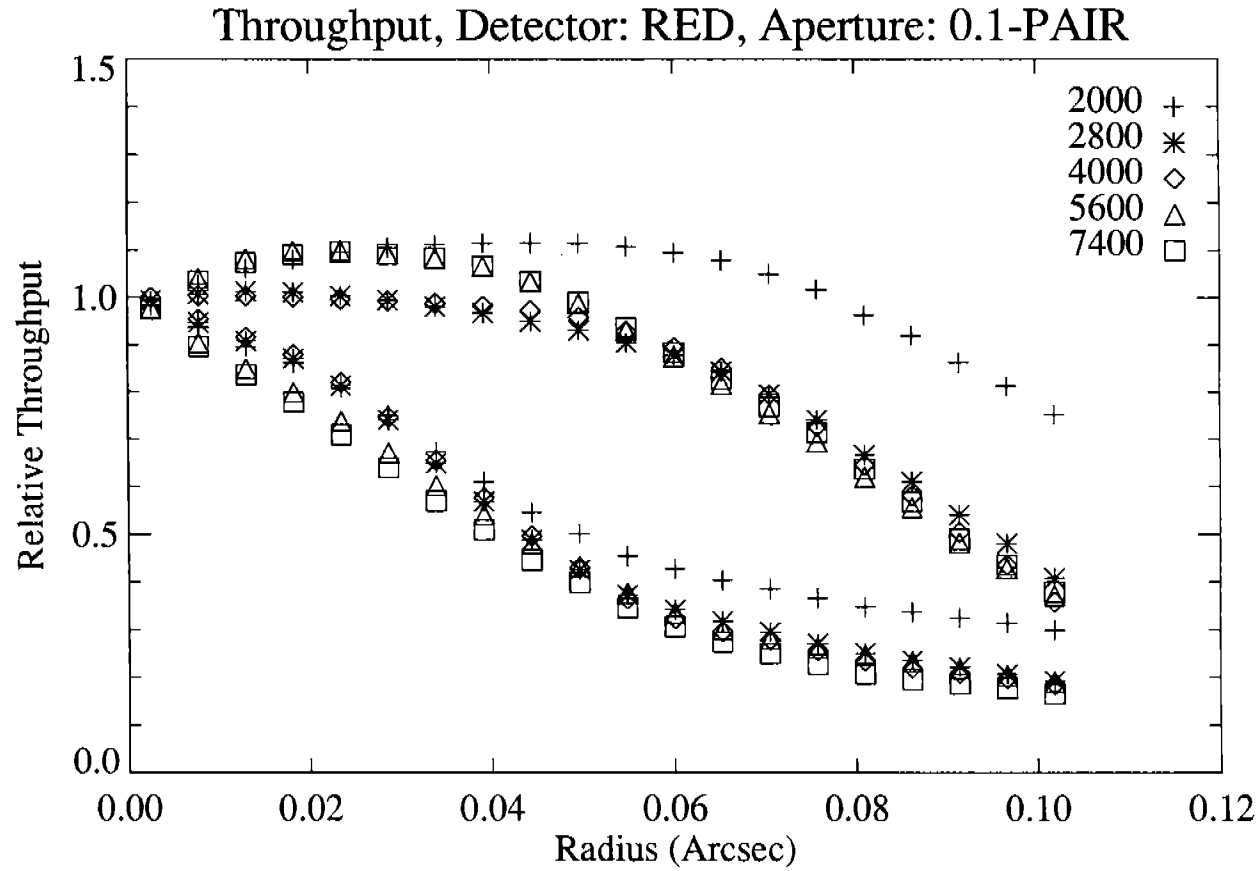

Figure 1 (Continued)

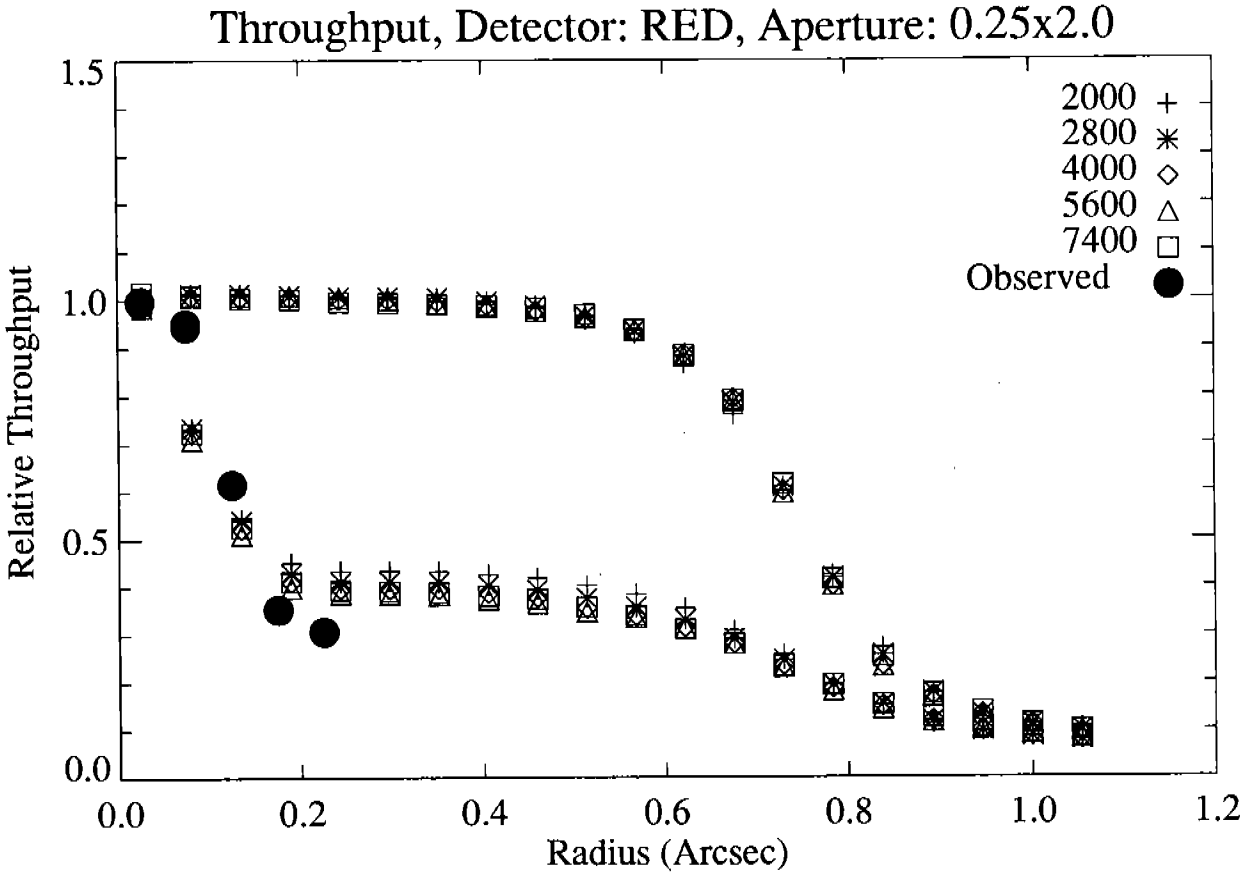

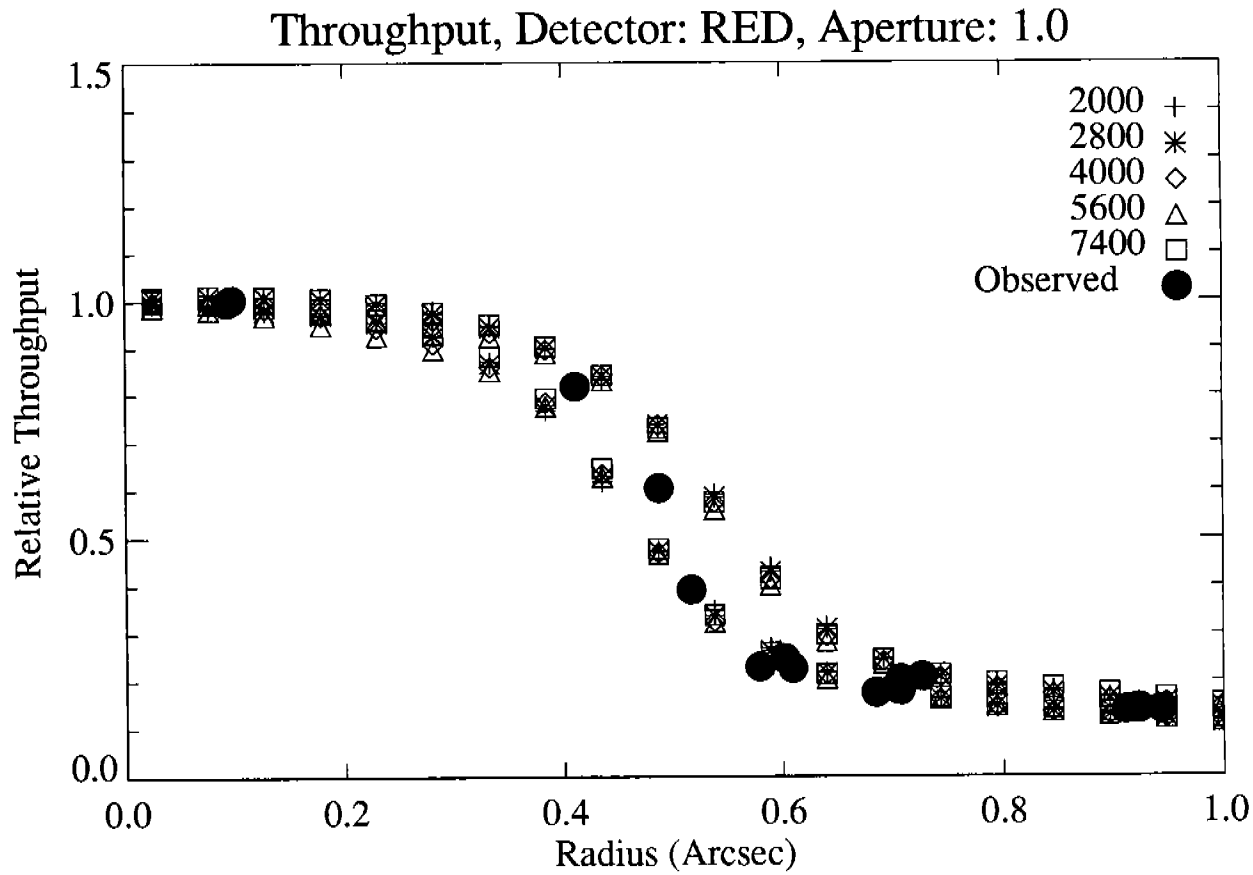

Figure 1 (Continued)

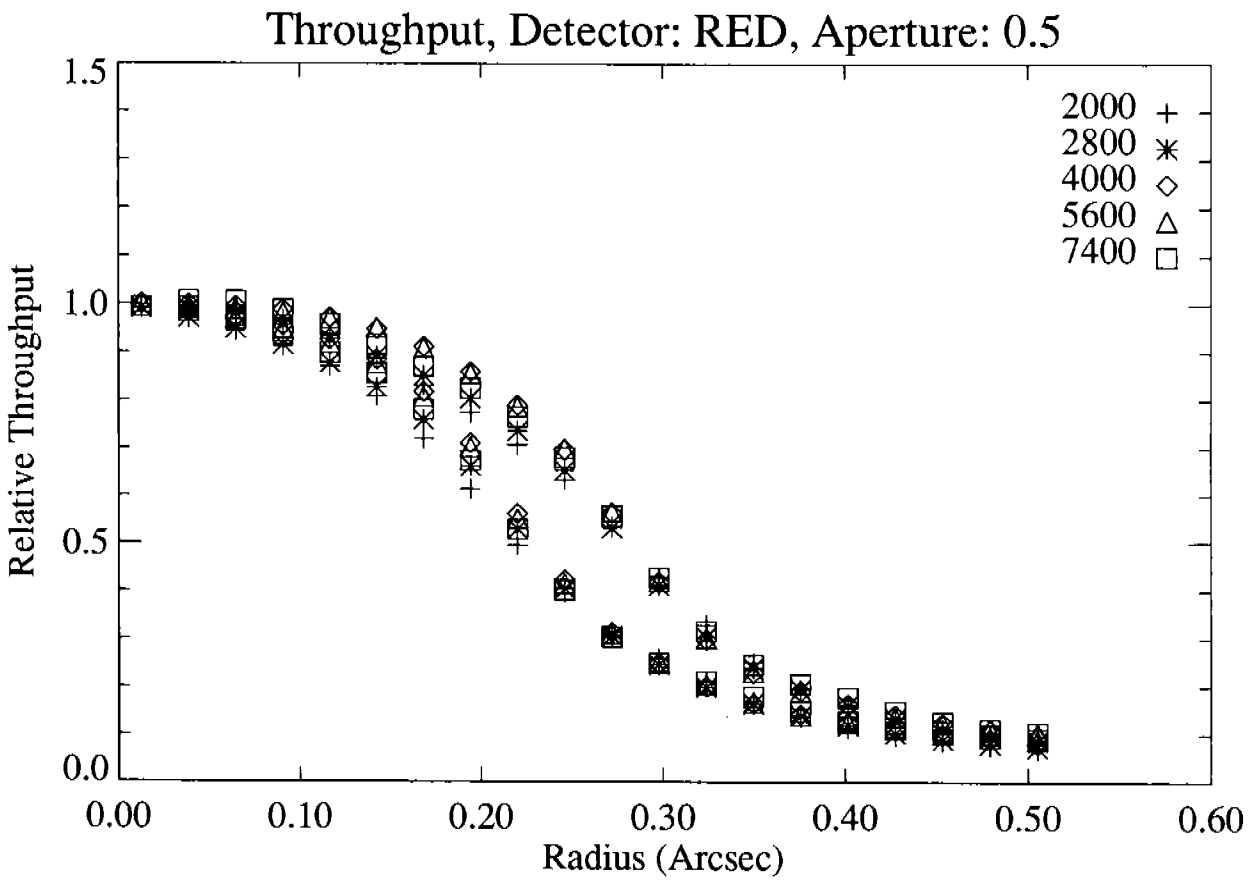

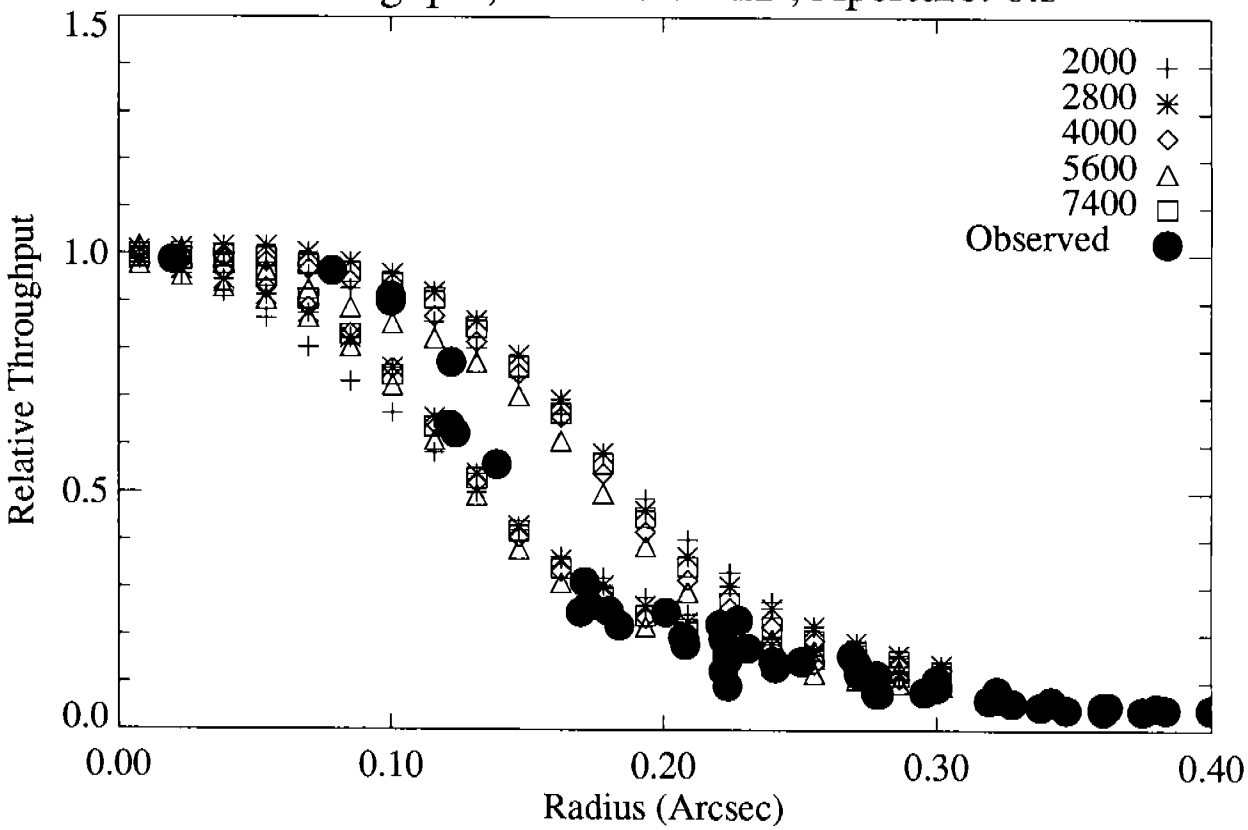

Figure 1 (Continued)

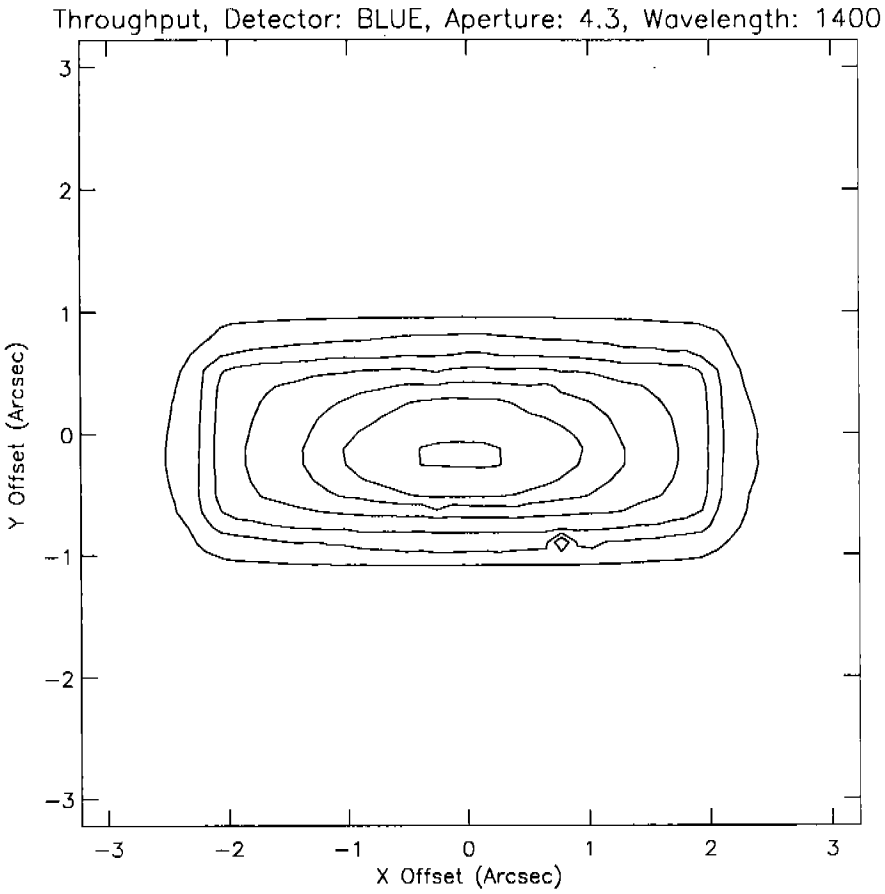
Throughput, Detector: BLUE, Aperture: 4.3, Wavelength: 1400
Y Offset (Arcsec)
X Offset (Arcsec)
3
2
1
0
−1
−2
−3
−3
−2
−1
0
1
2
3

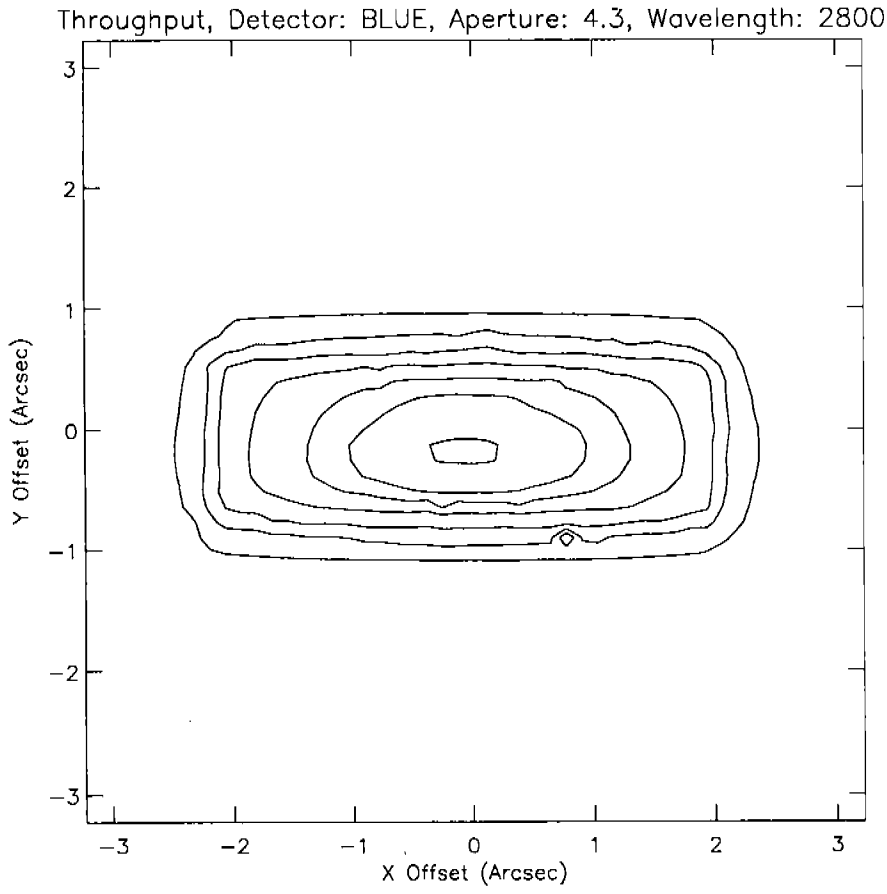
Throughput, Detector: BLUE, Aperture: 4.3, Wavelength: 2800
Y Offset (Arcsec)
X Offset (Arcsec)
3
2
1
0
−1
−2
−3
−3
−2
−1
0
1
2
3

Figure 2

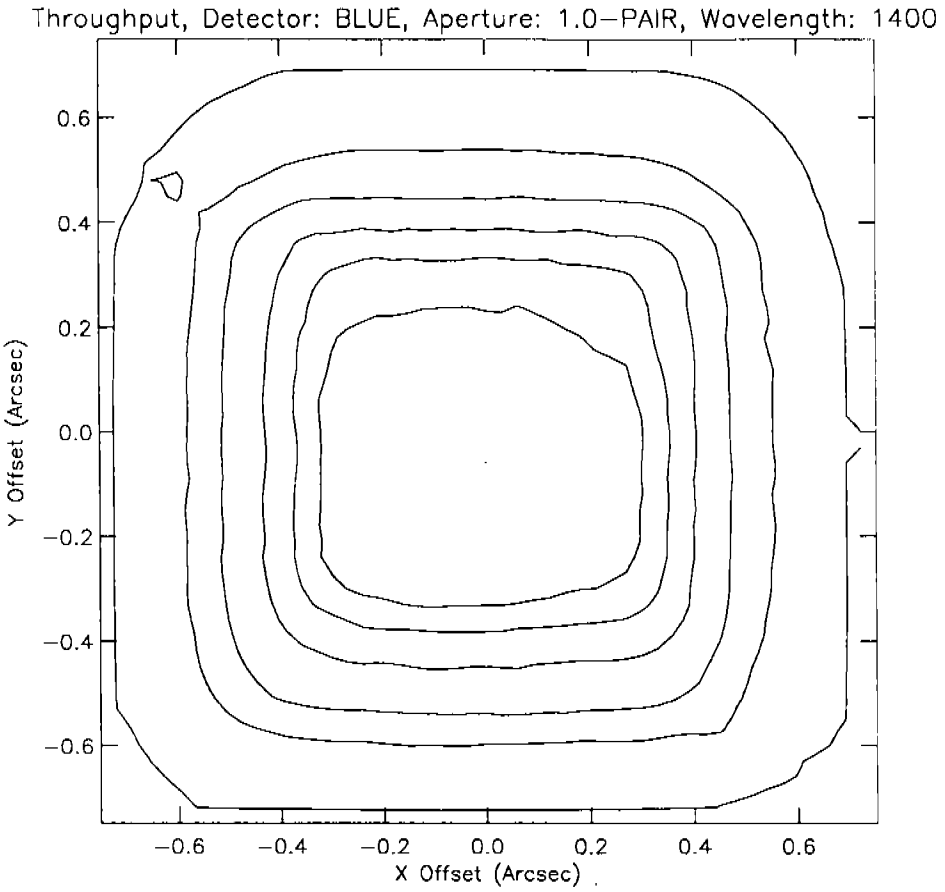

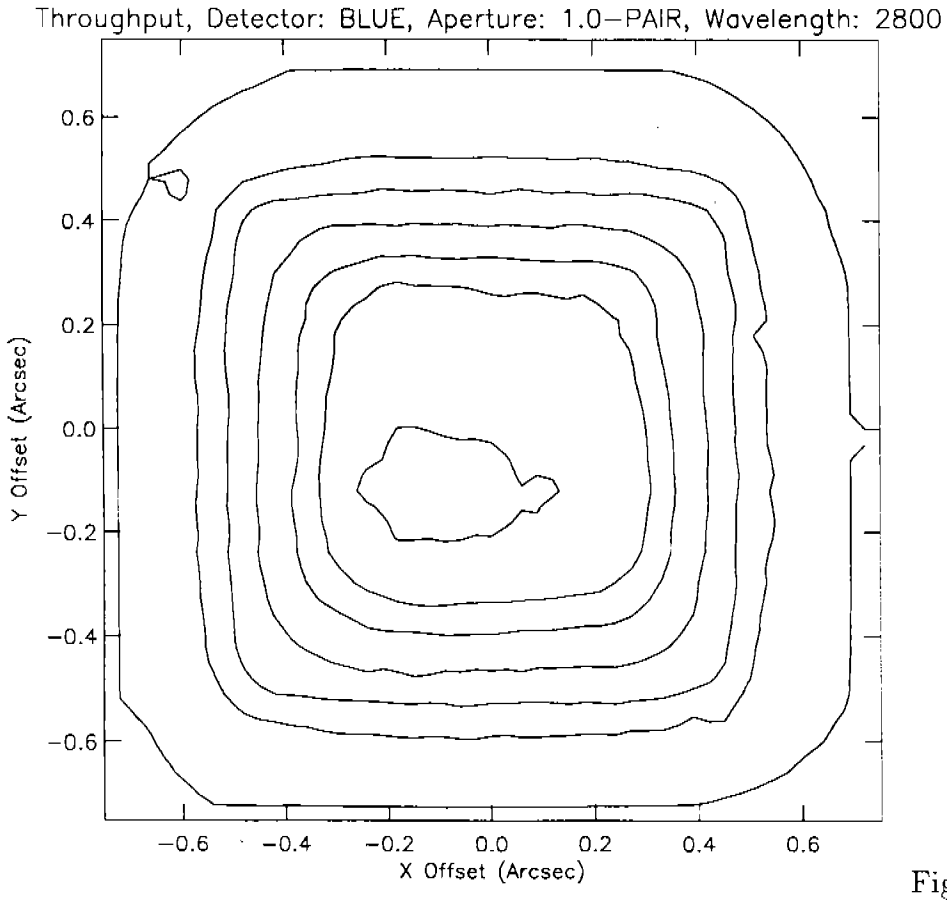

Figure 2 (Continued)

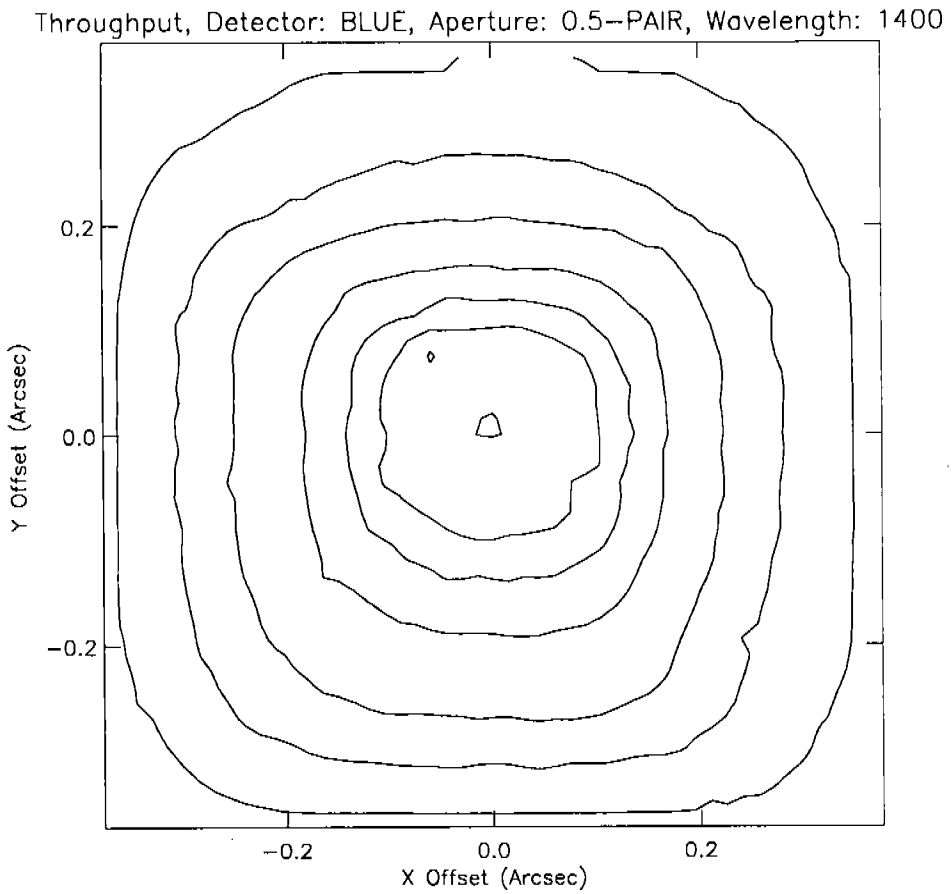

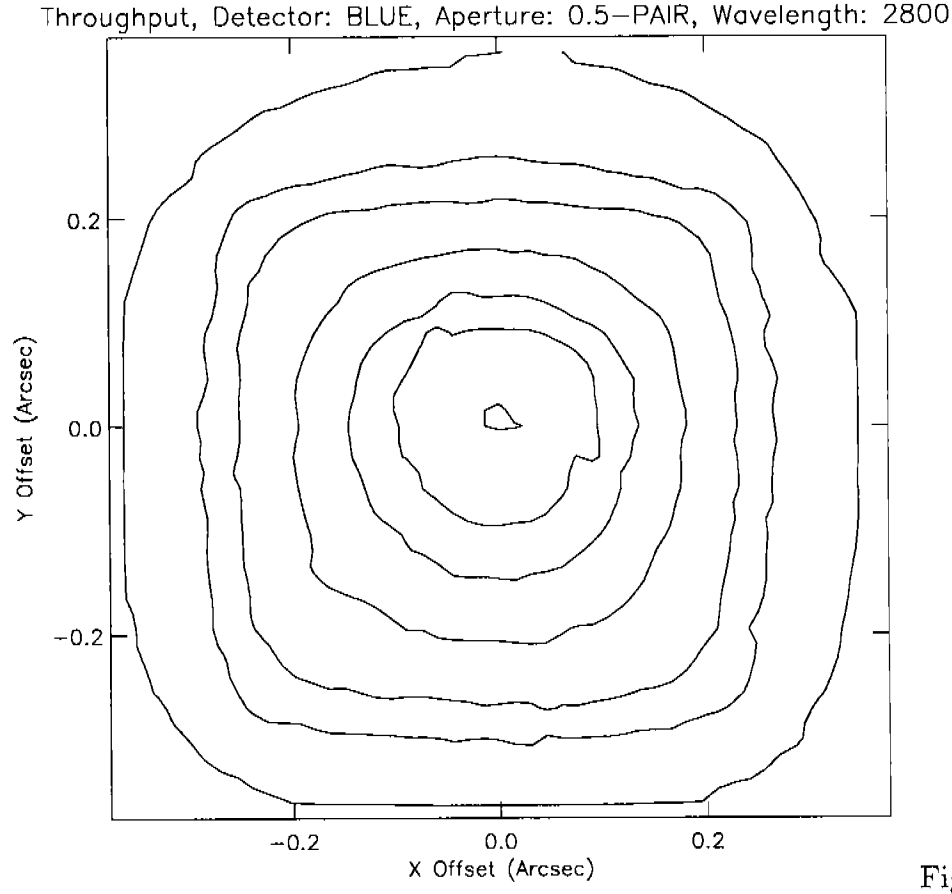

Figure 2 (Continued)

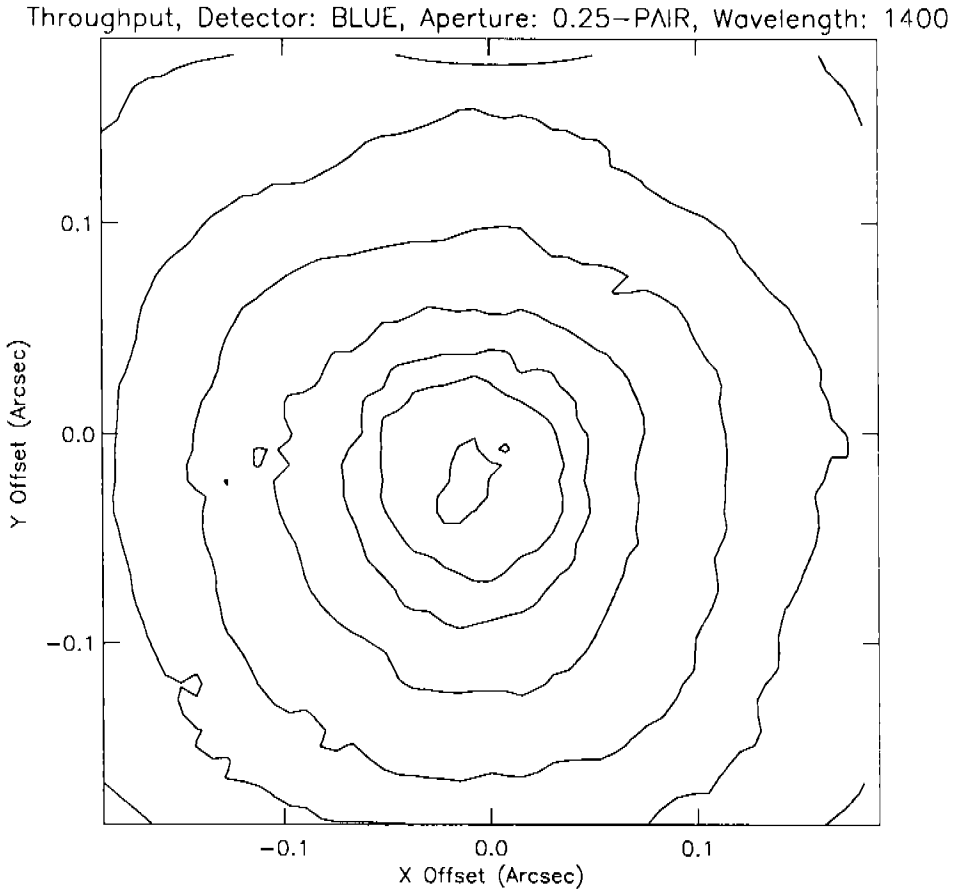

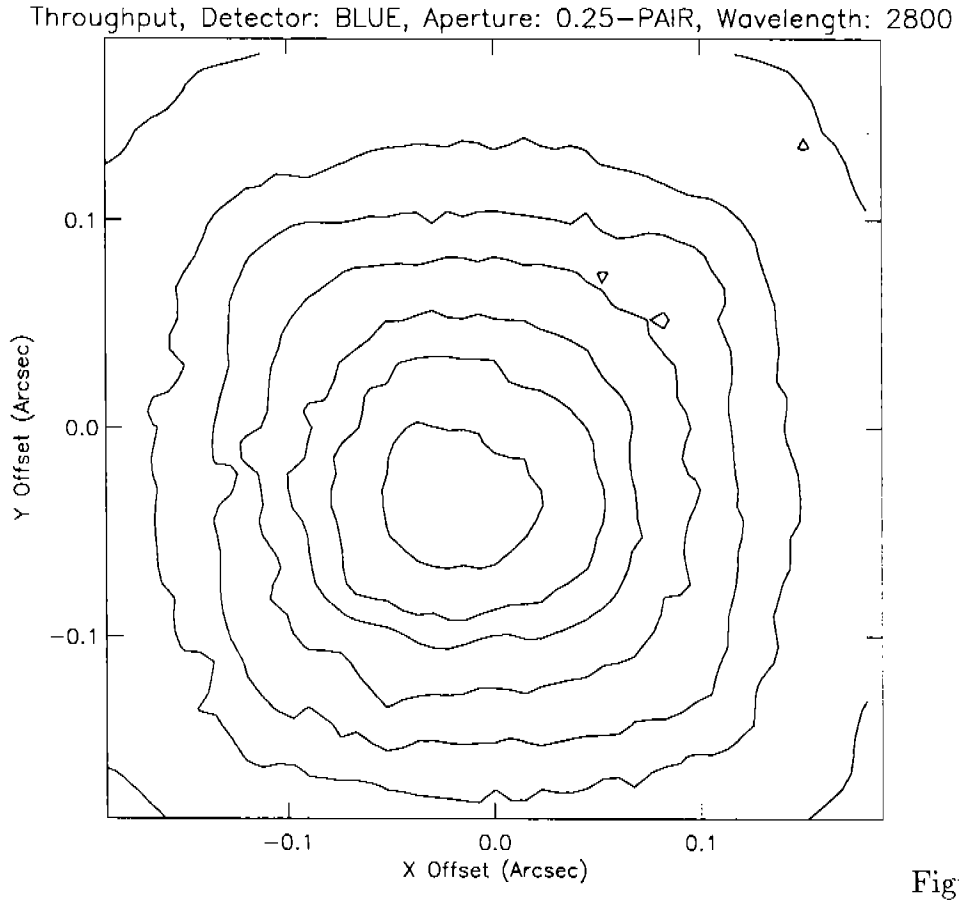

Figure 2 (Continued)

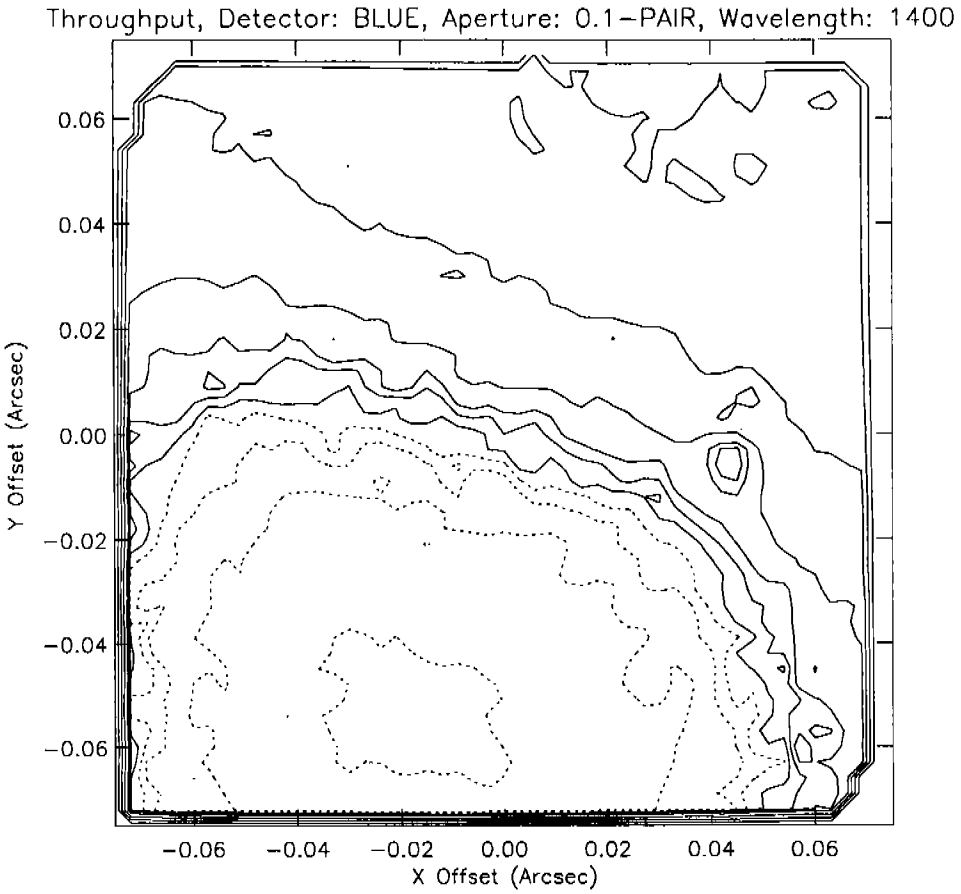

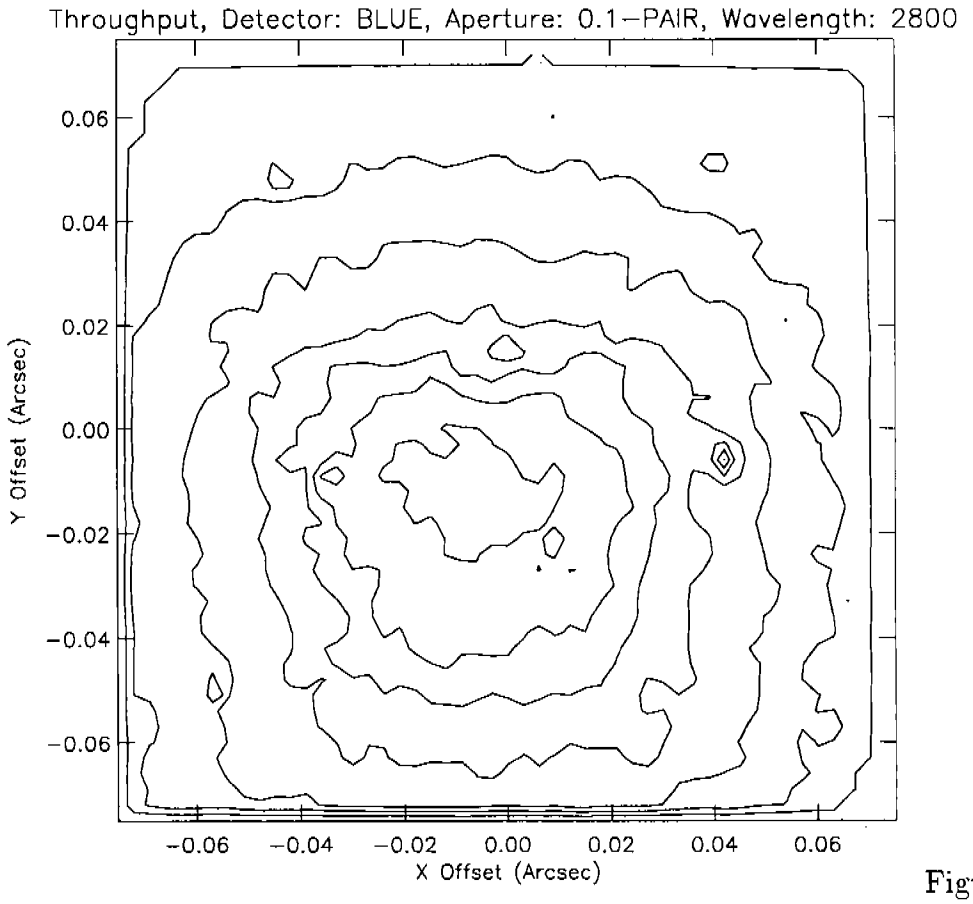

Figure 2 (Continued)

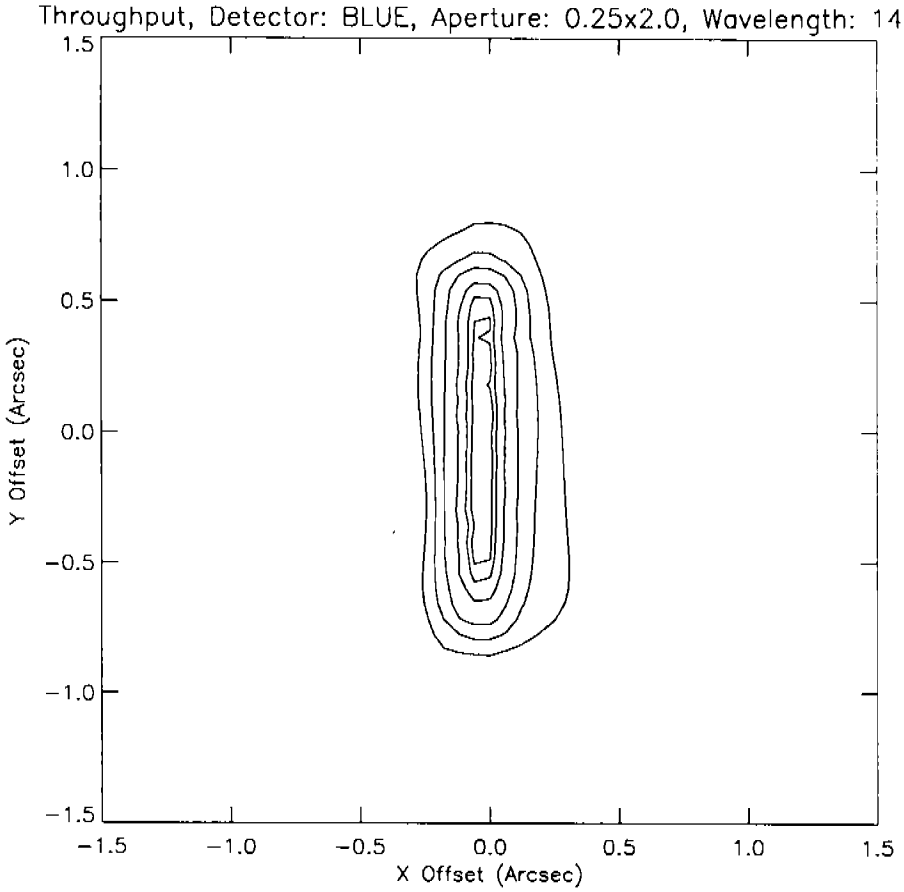

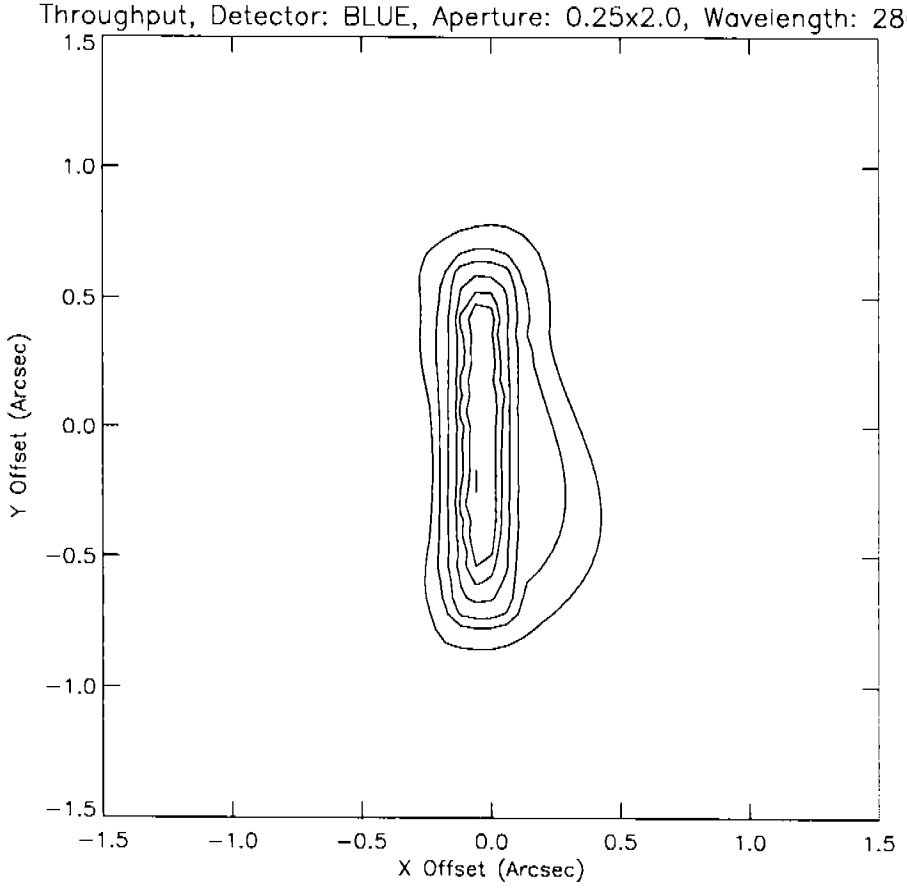

Figure 2 (Continued)

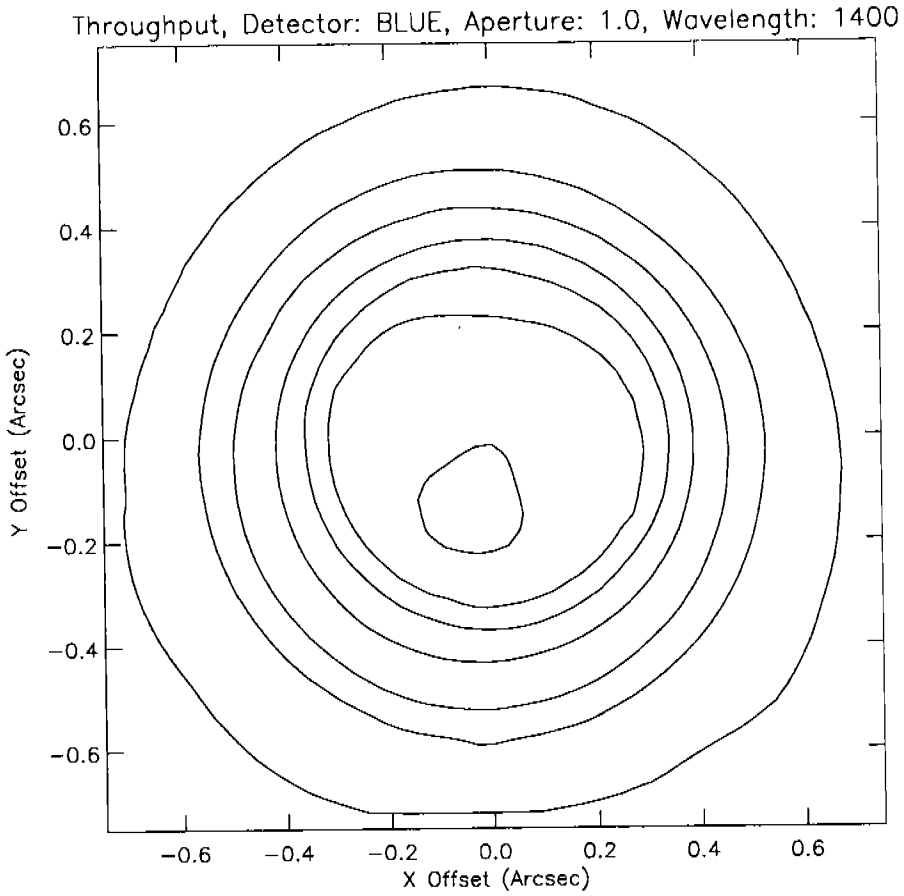

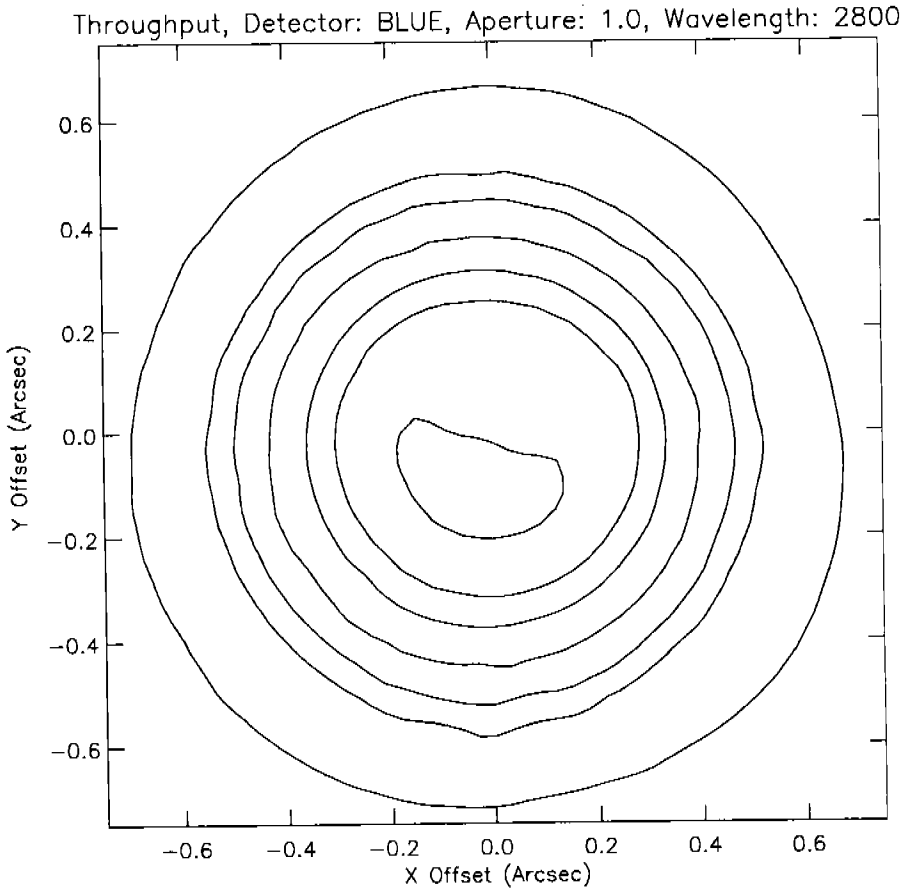

Figure 2 (Continued)

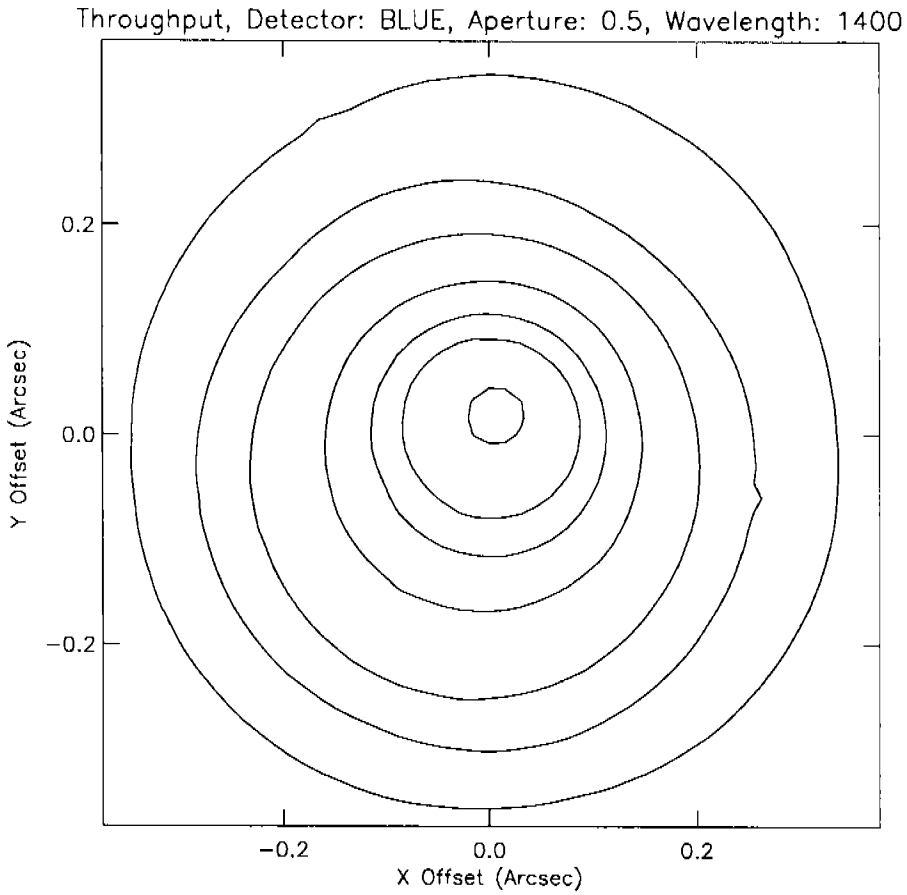

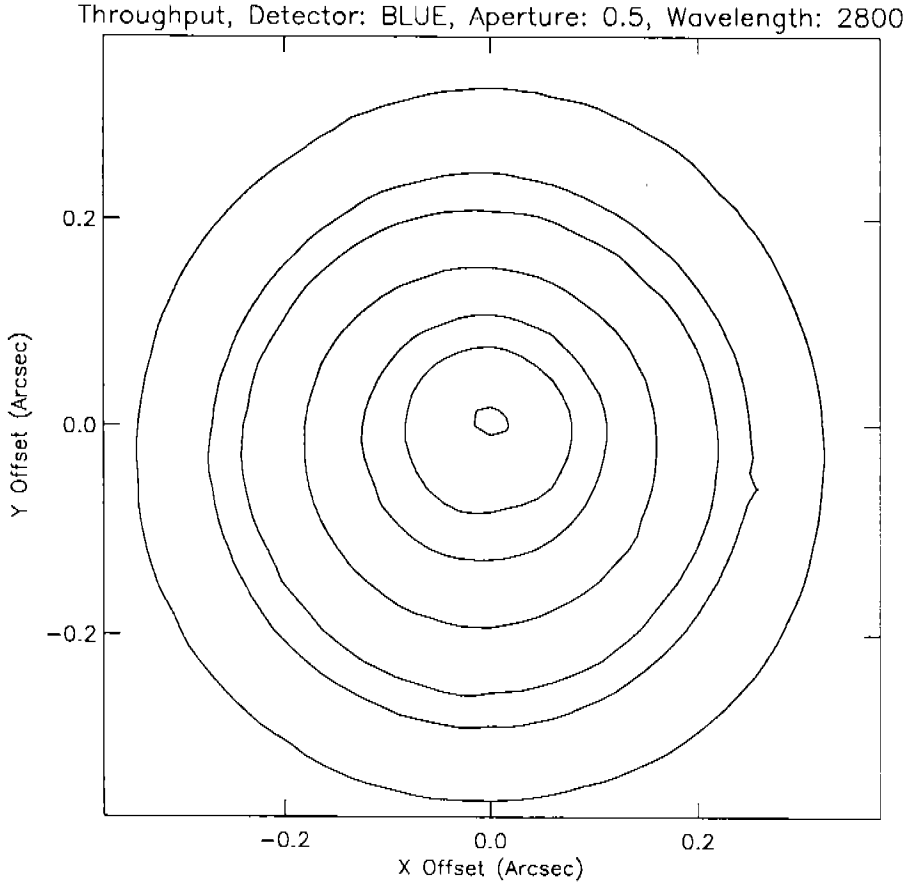

Figure 2 (Continued)

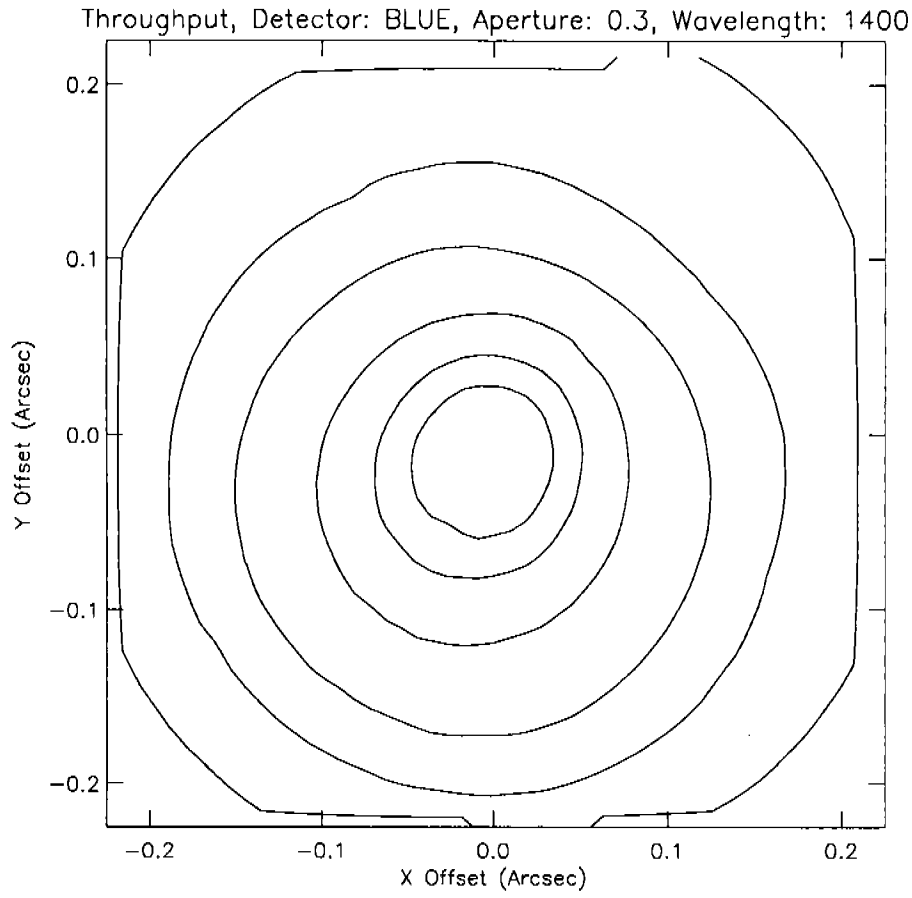

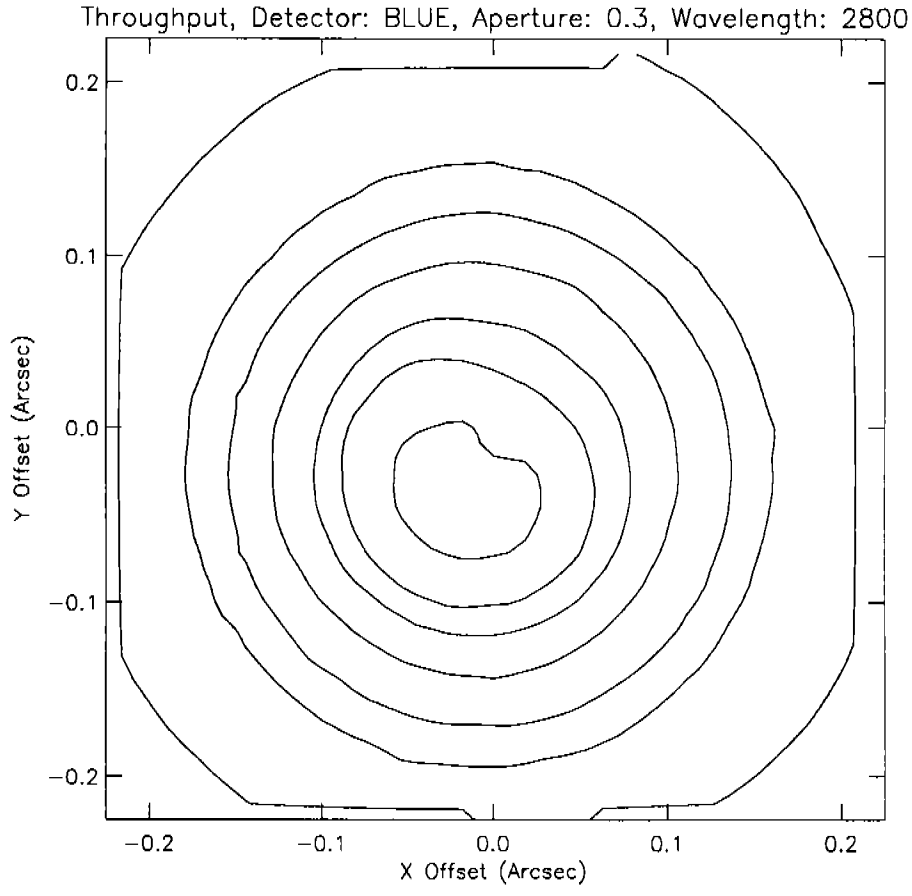

Figure 2 (Continued)

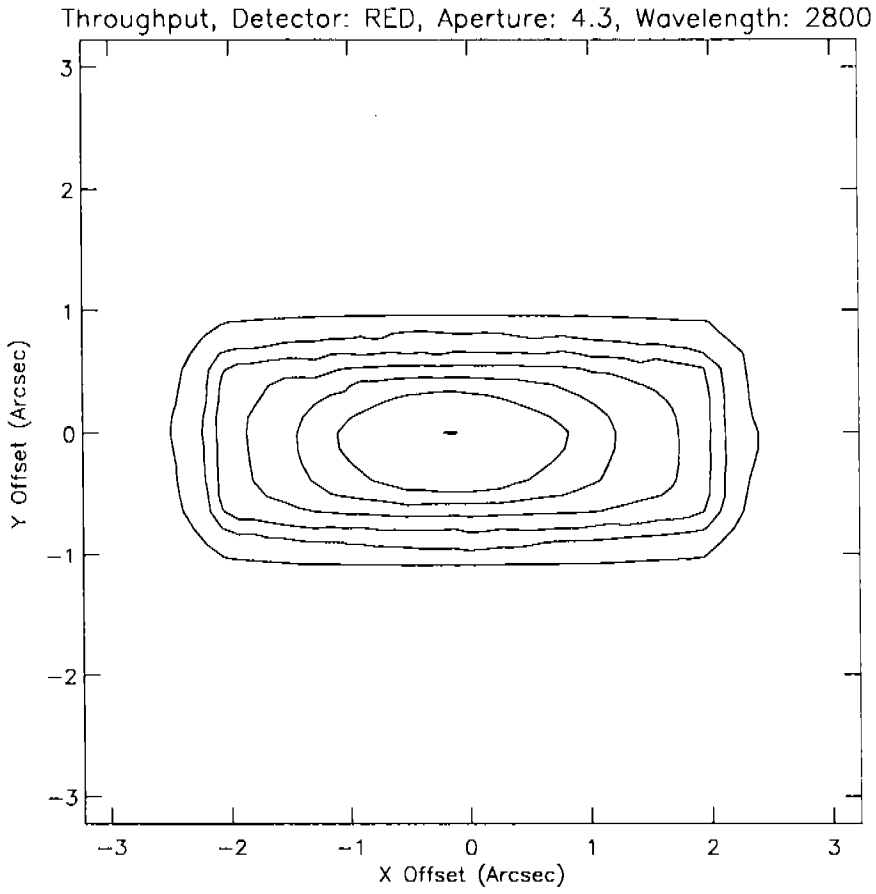

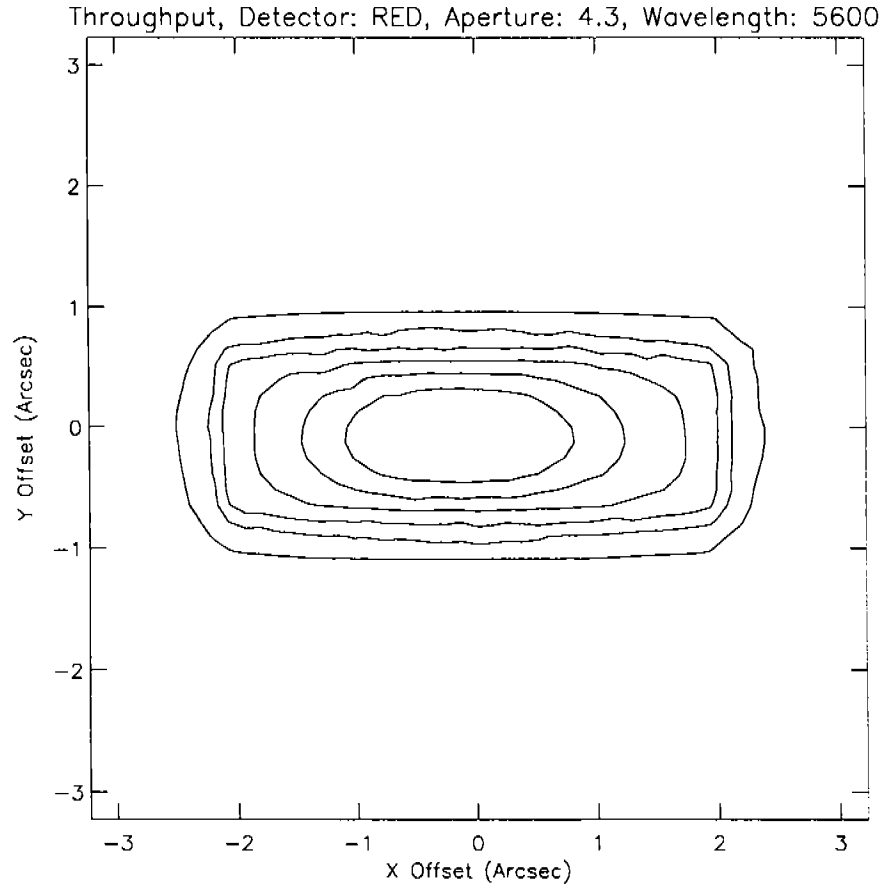

Figure 2 (Continued)

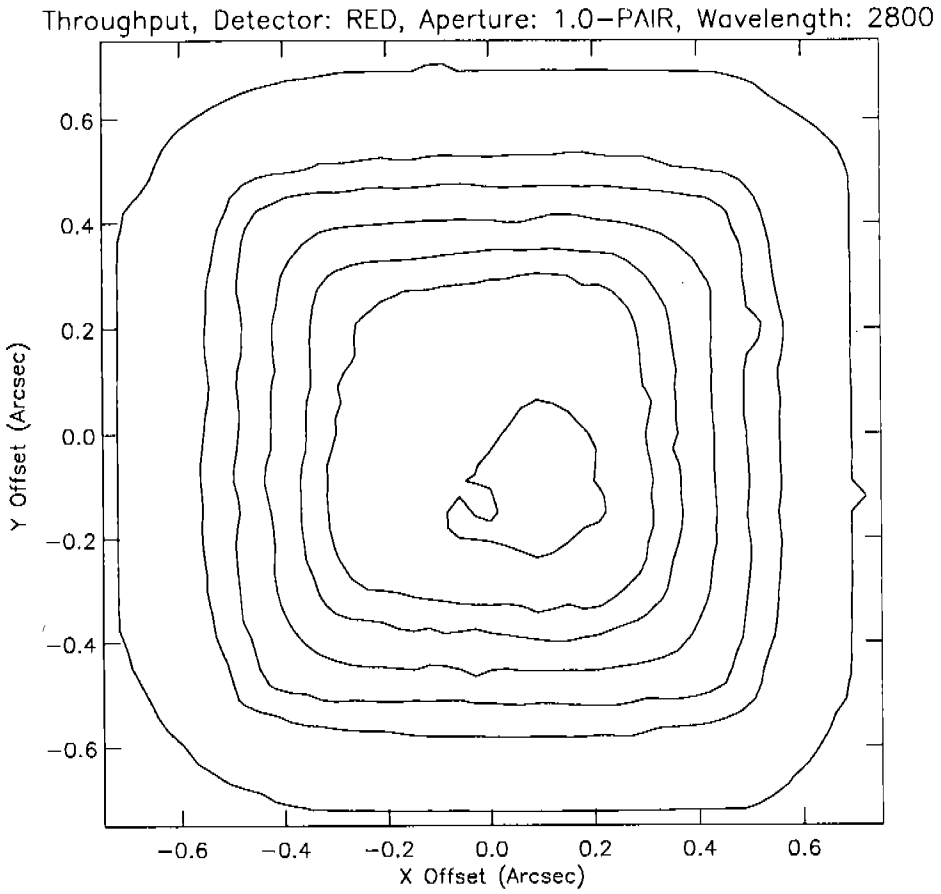

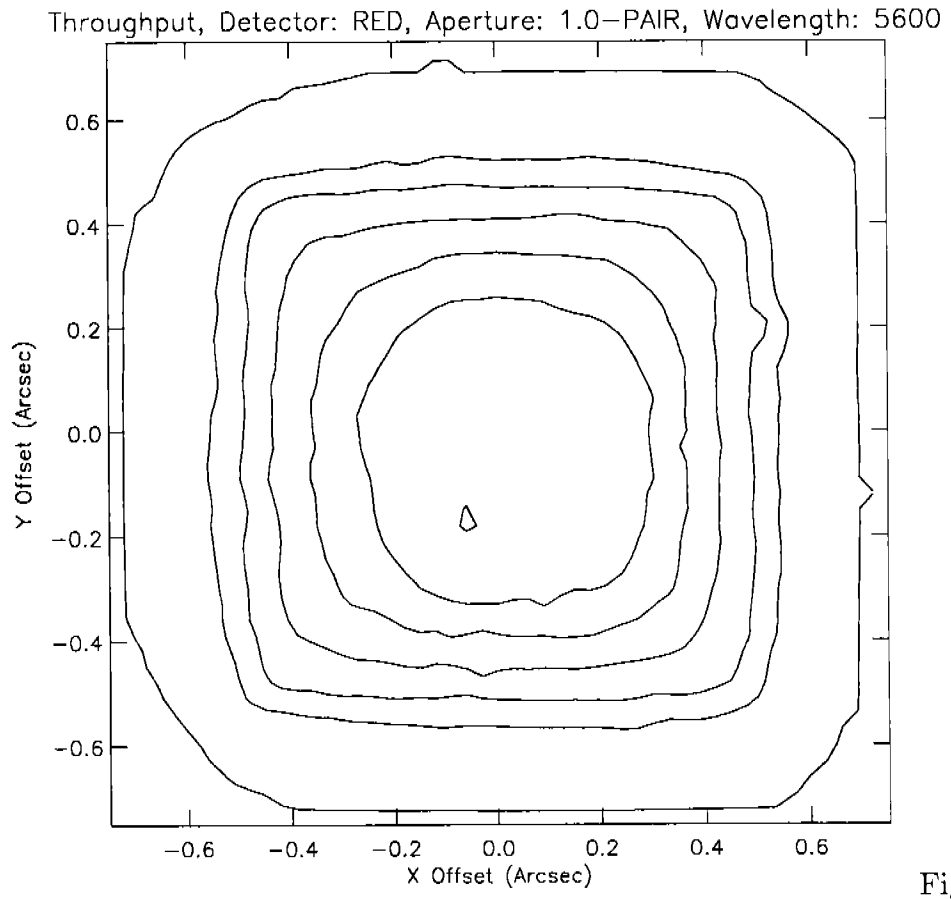

Figure 2 (Continued)

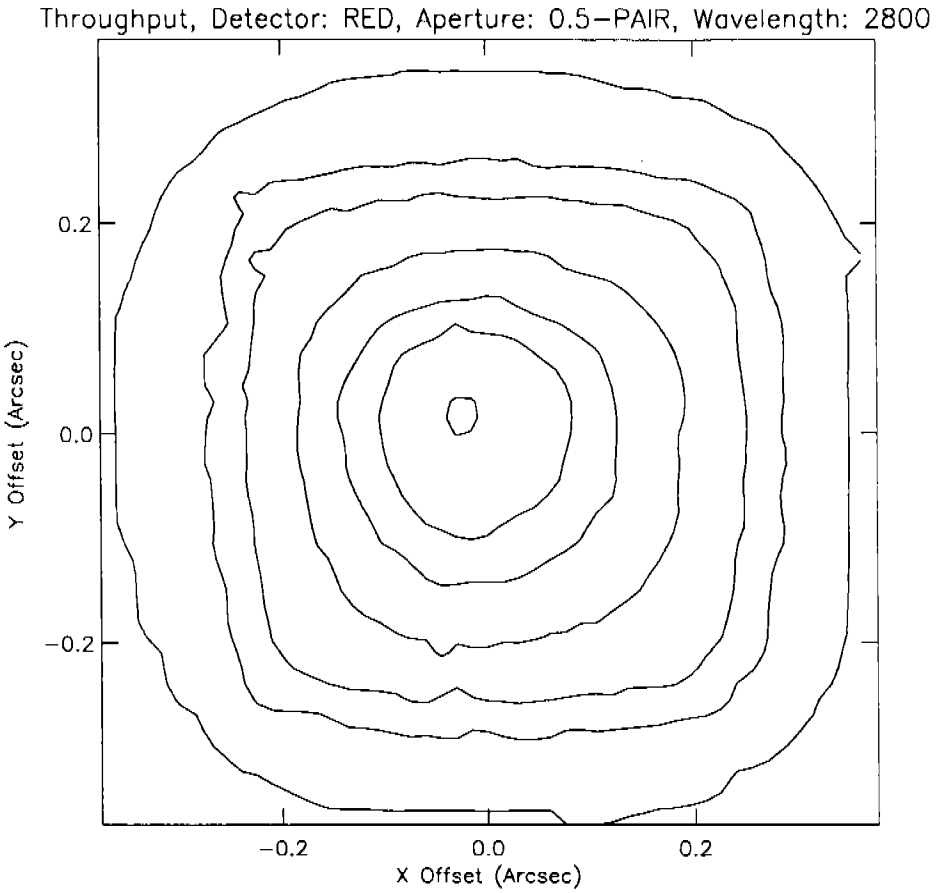

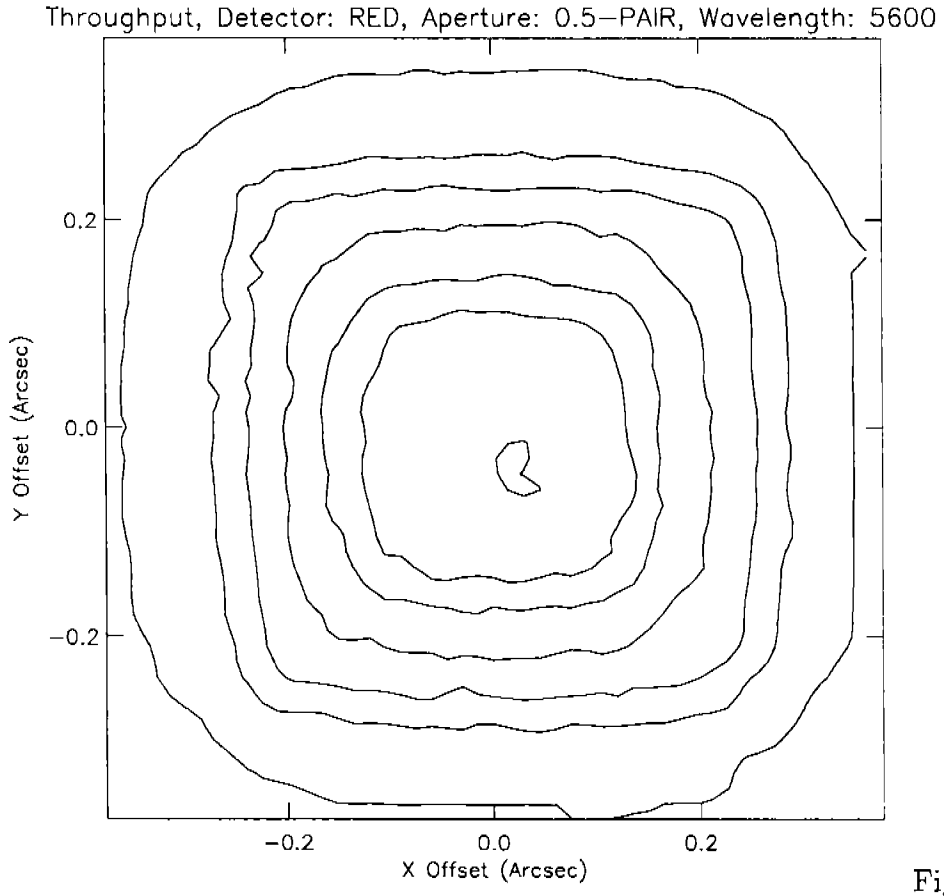

Figure 2 (Continued)

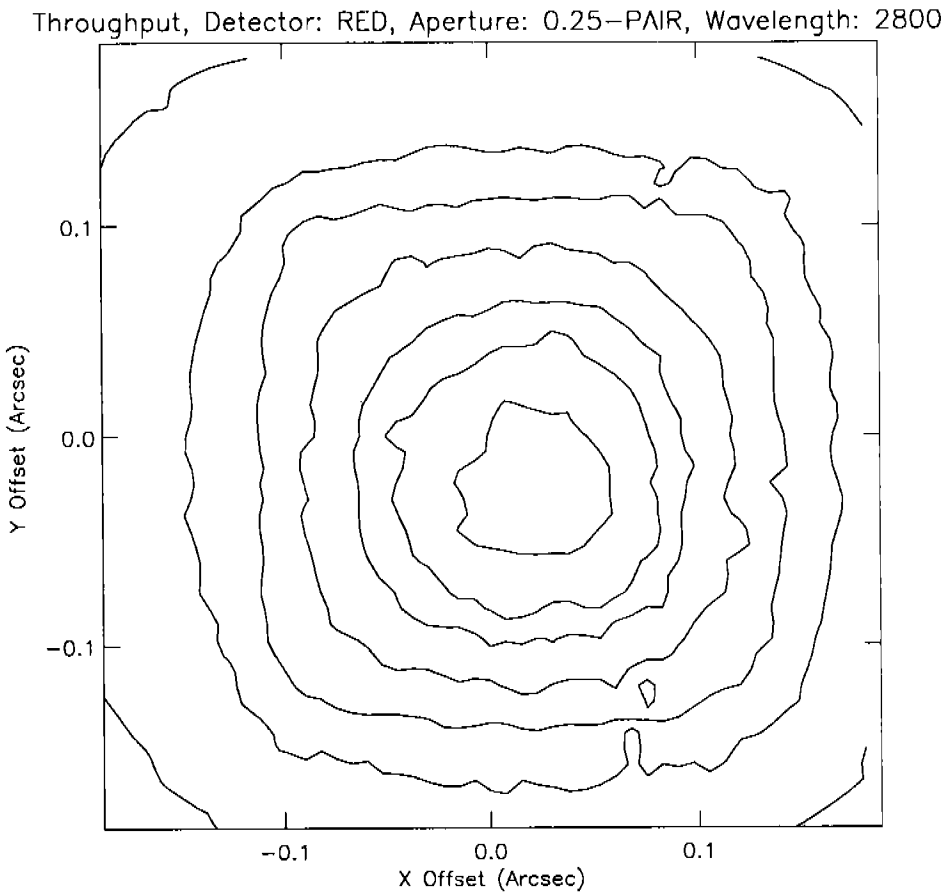

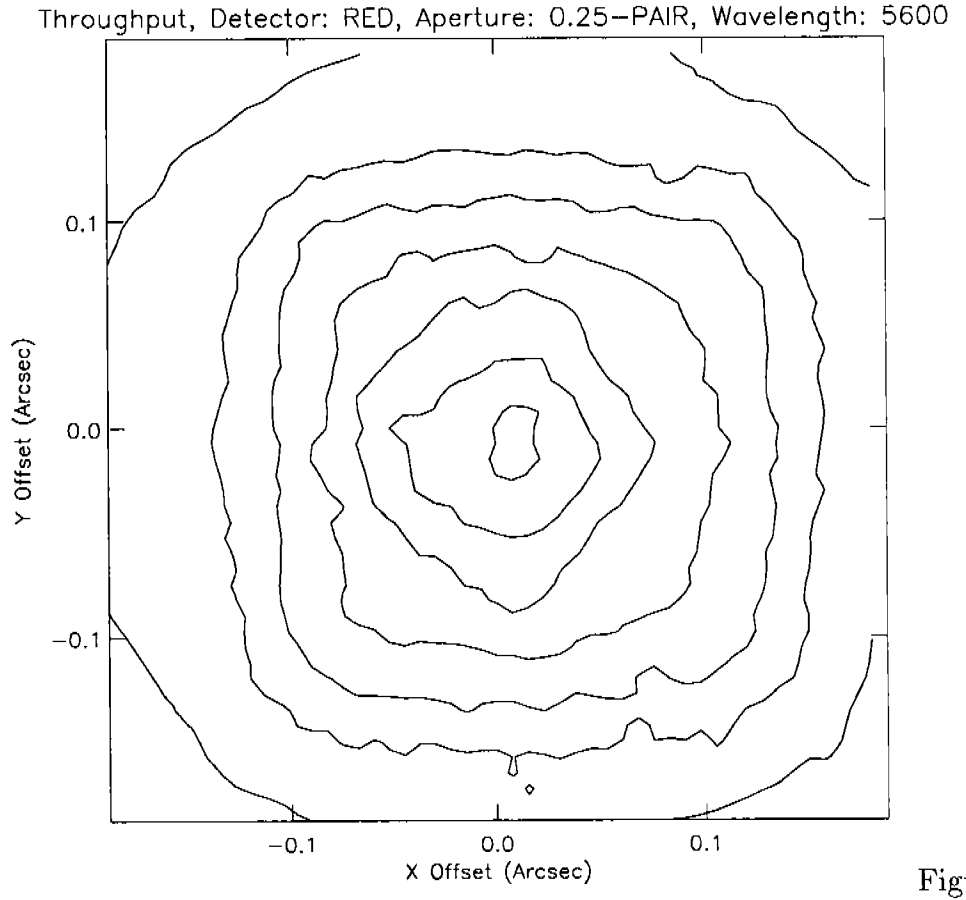

Figure 2 (Continued)

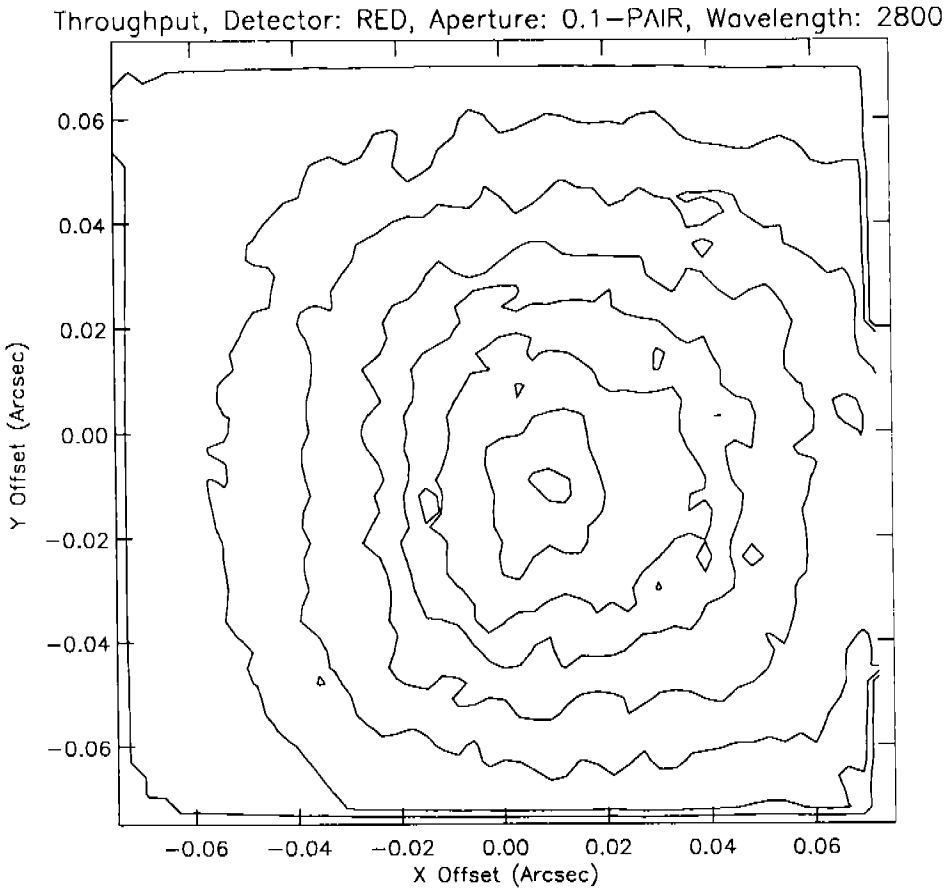

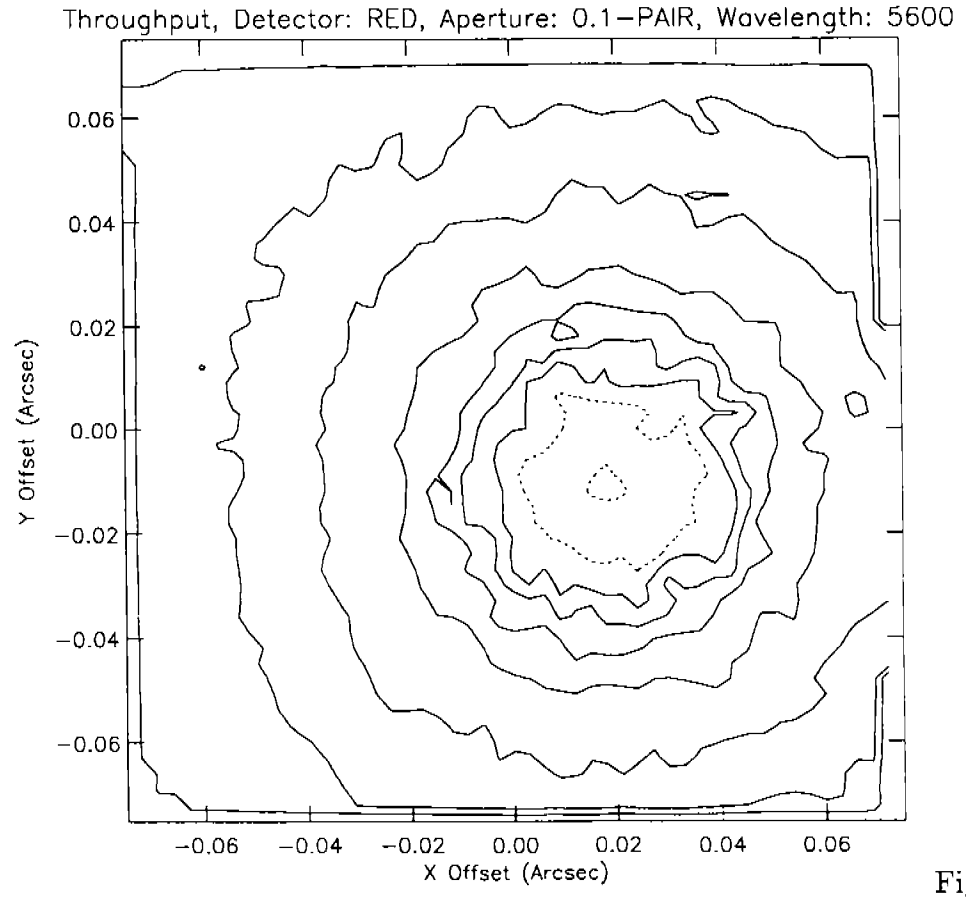

Figure 2 (Continued)

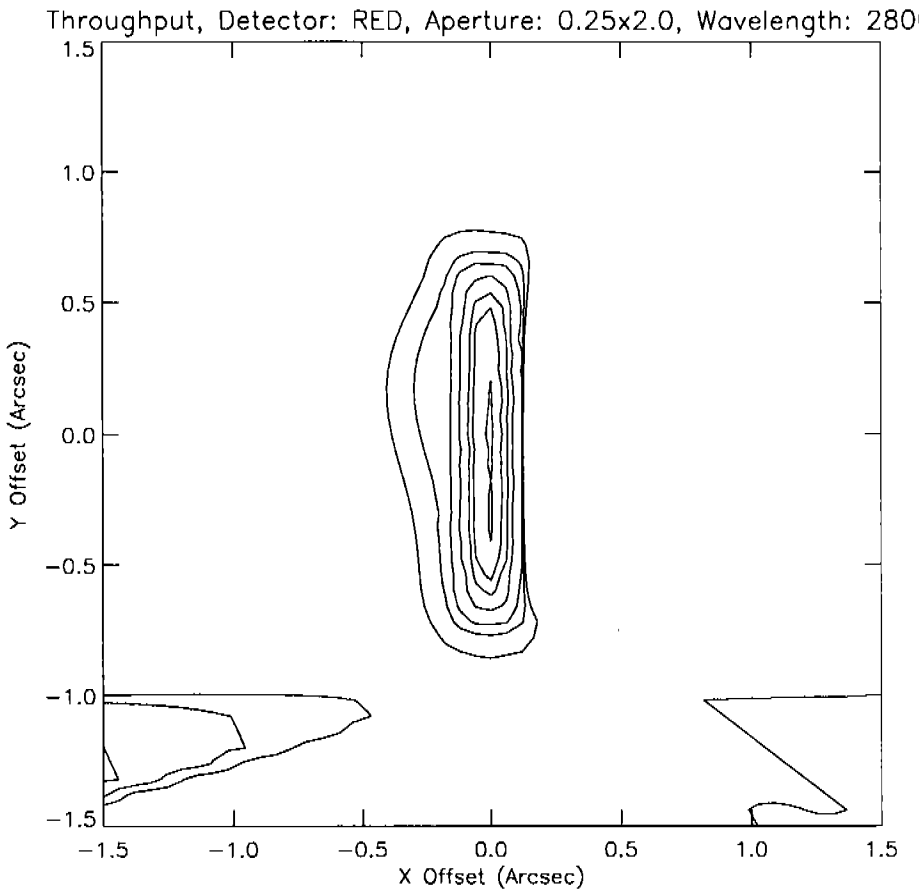

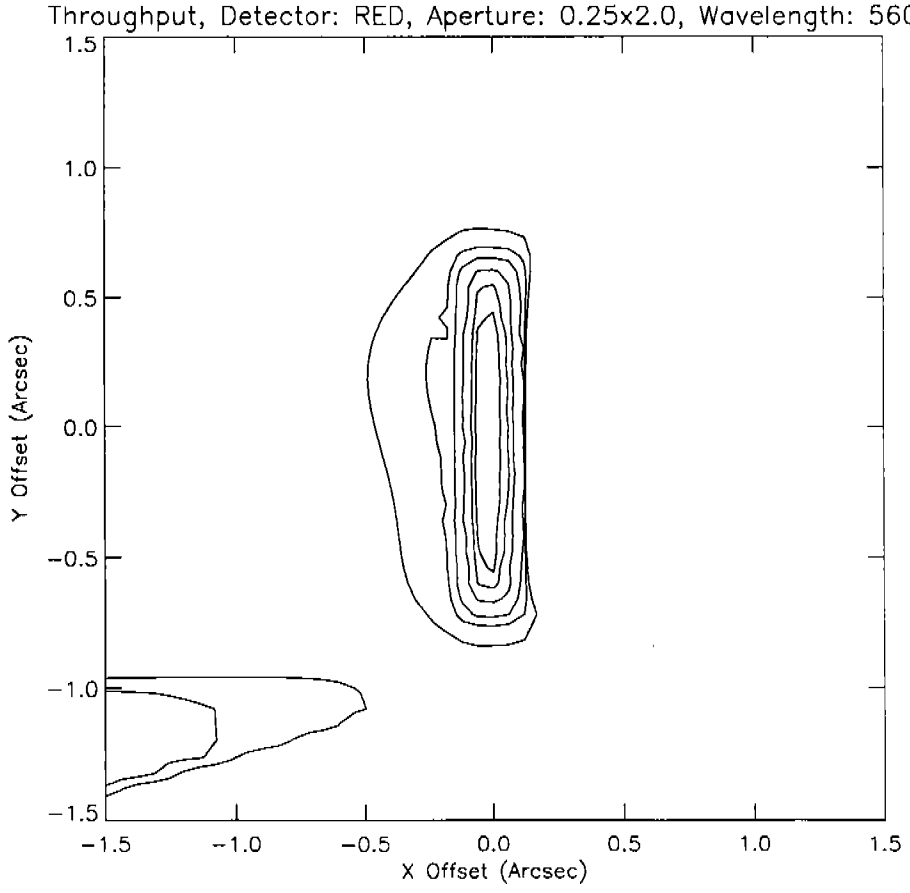

Figure 2 (Continued)

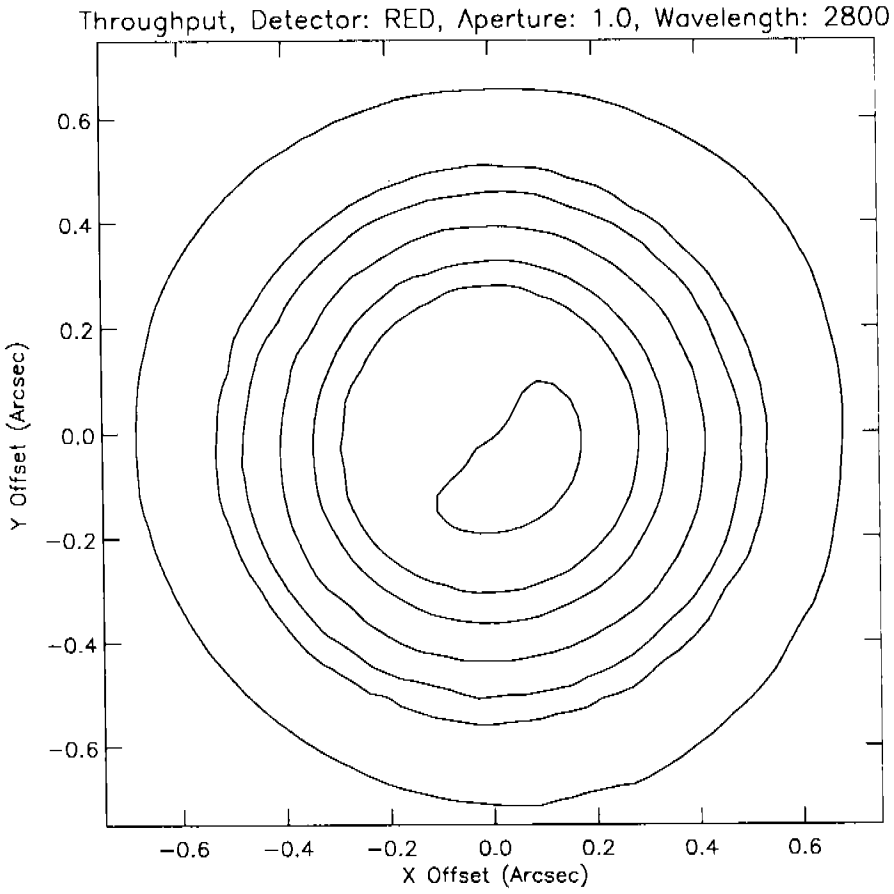

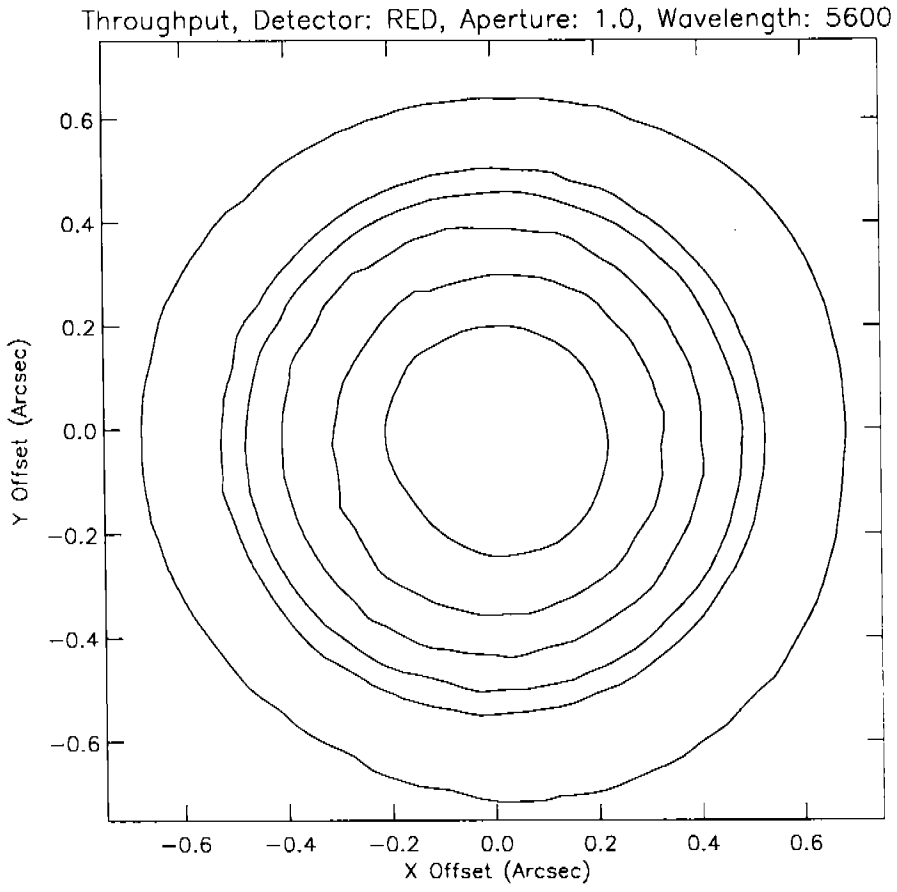

Figure 2 (Continued)

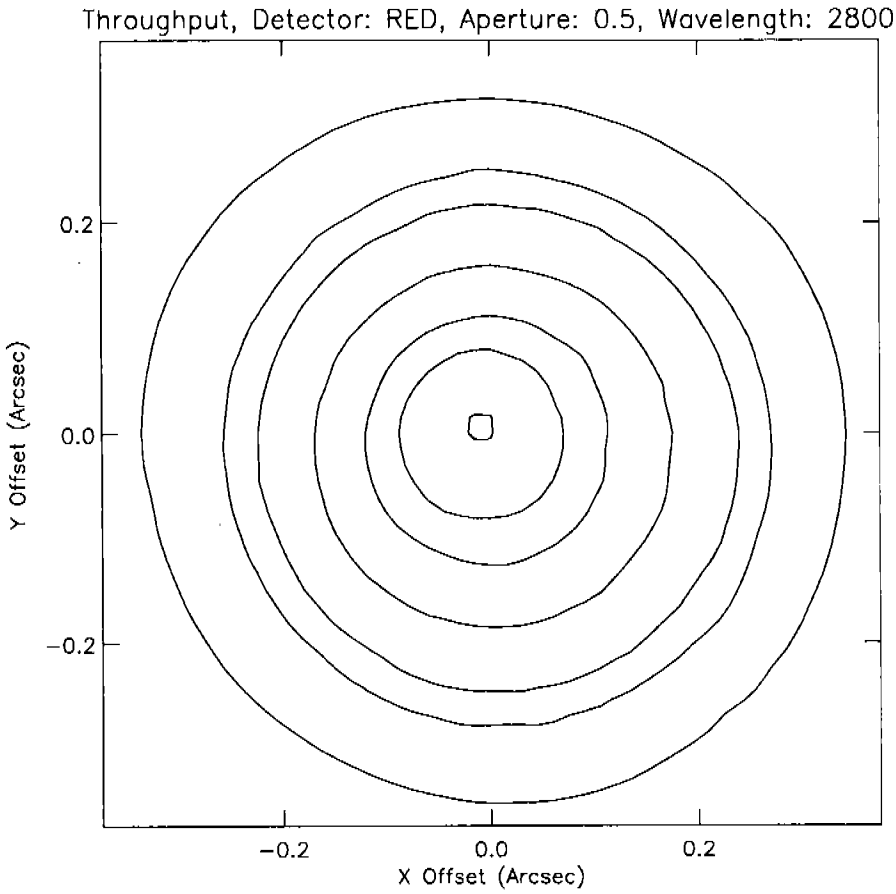

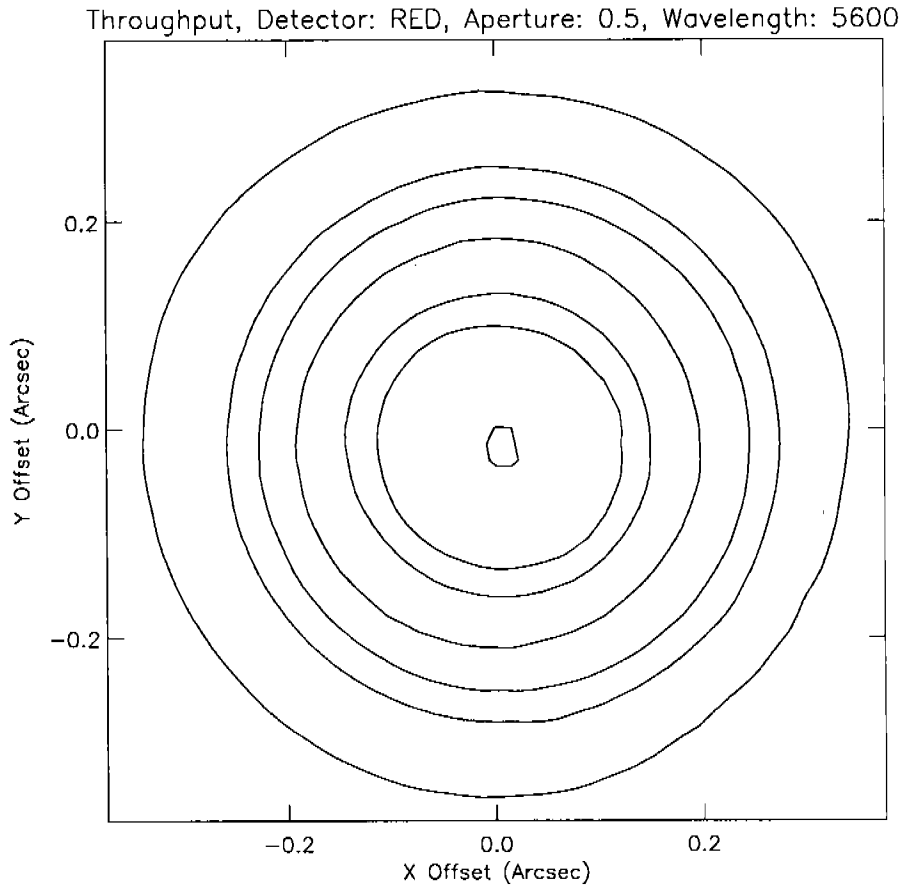

Figure 2 (Continued)

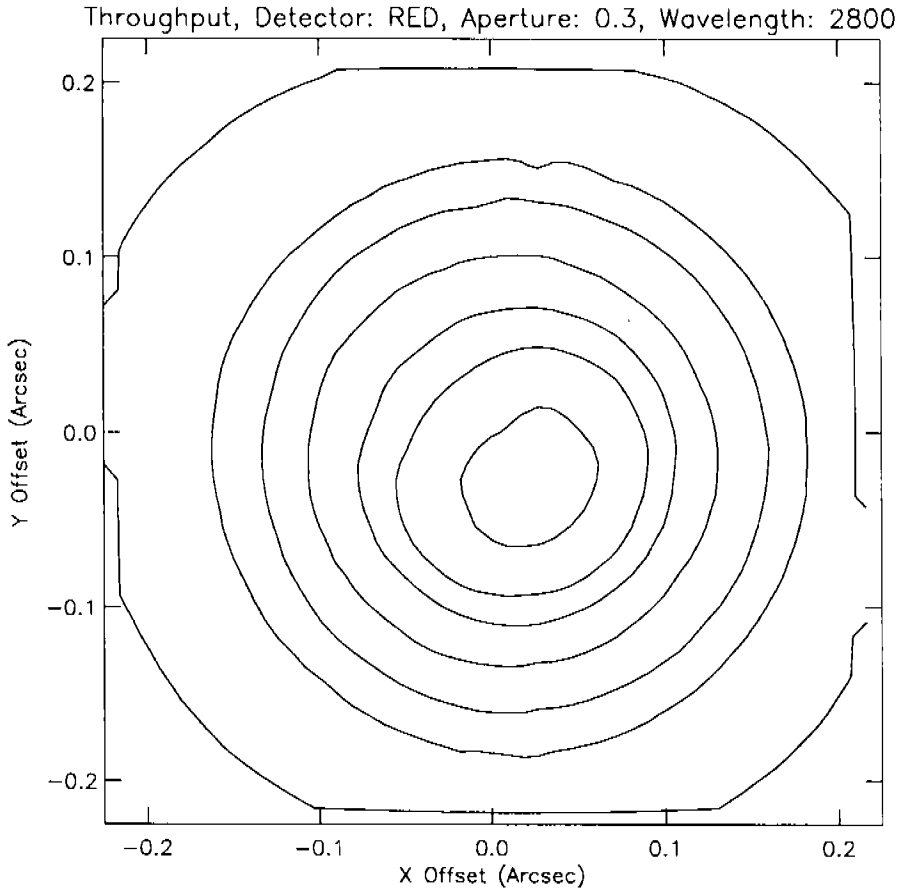

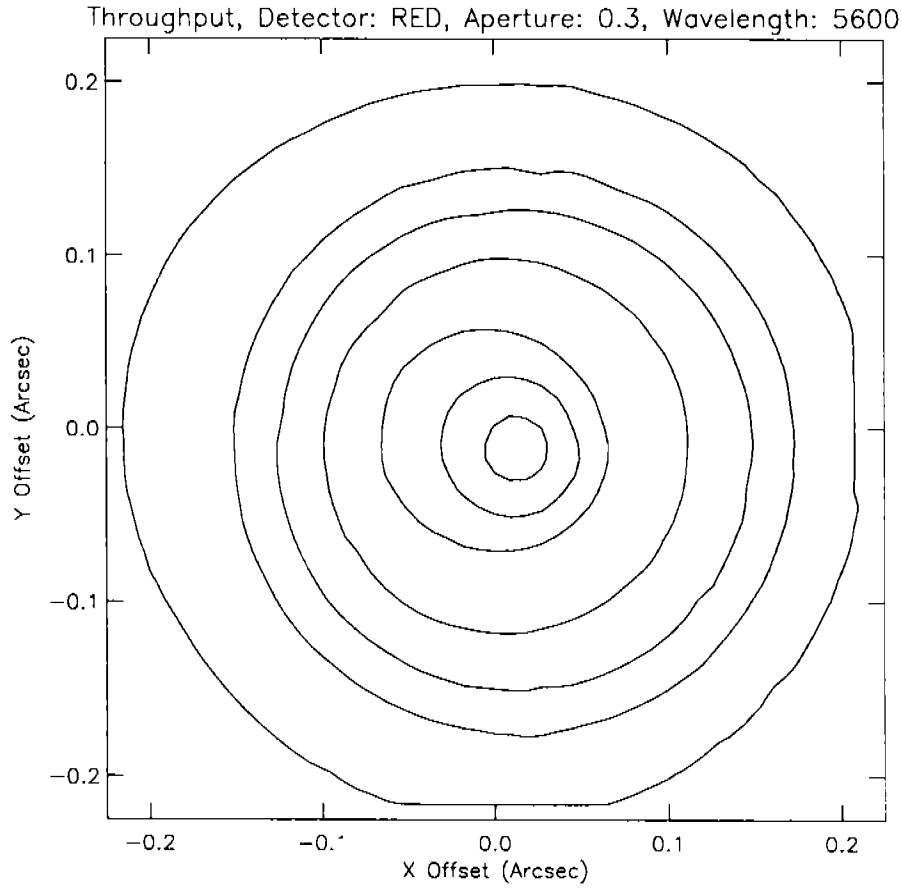

Figure 2 (Continued)